AD-A151 990 METALLURGICAL CHARACTERIZATION OF ALUMINUM POWDER CONSOLIDATION(U) MCDONNELL DOUGLAS RESEARCH LABS ST LOUIS MO S M SASTRY ET AL. SEP 84 AFOSR-TR-85-0254 1/1

UNCLASSIFIED F49620-83-C-0152 F/G 11/6 NL

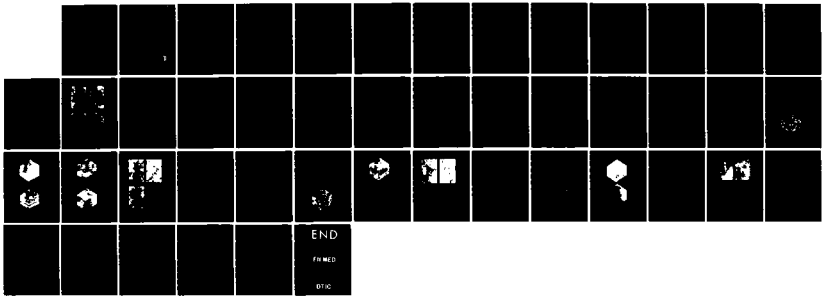

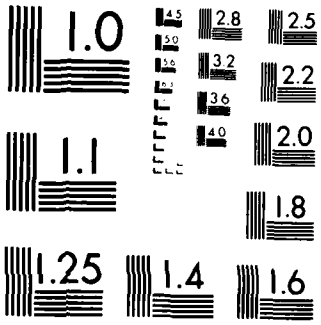

MICROCOPY RESOLUTION TEST CHART
NATIONAL BUREAU OF STANDARDS 1963 A

AFOSR-TR- 85-0254

AD-A151 990

METALLURGICAL CHARACTERIZATION OF ALUMINUM POWDER CONSOLIDATION

S. M. L. Sastry
T. C. Peng
D. M. Bowden
J. E. O'Neal

McDonnell Douglas Research Laboratories
St. Louis, Missouri 63166

September 1984
Annual Technical Report for the Period 1 September 1983 - 1 September 1984

Approved for public release; distribution unlimited

DTIC FILE COPY

The views and conclusions contained in this document are those of the authors and should not be interpreted as necessarily representing the official policies or endorsements, either expressed or implied, of the Air Force Office of Scientific Research of the U.S. Government.

DTIC
ELECTE
MAR 28 1985
S D
E

Prepared for:

UNITED STATES AIR FORCE
Air Force Office of Scientific Research
Bolling Air Force Base, DC 20332

85 03 12 083

UNCLASSIFIED

SECURITY CLASSIFICATION OF THIS PAGE (When Data Entered)

Caplan

REPORT DOCUMENTATION PAGE		READ INSTRUCTIONS BEFORE COMPLETING FORM
1. REPORT NUMBER AFOSR-TR- 85-0254	2. GOVT ACCESSION NO. AD A151 990	3. RECIPIENT'S CATALOG NUMBER
4. TITLE (and Subtitle) METALLURGICAL CHARACTERIZATION OF ALUMINUM POWDER CONSOLIDATION		5. TYPE OF REPORT & PERIOD COVERED Annual technical report 1 Sep. 1983-1 Sep. 1984
		6. PERFORMING ORG. REPORT NUMBER
7. AUTHOR(s) S. M. L. Sastry, T. C. Peng, D. M. Bowden, and J. E. O'Neal		8. CONTRACT OR GRANT NUMBER(s) F49620-83-C-0152
9. PERFORMING ORGANIZATION NAME AND ADDRESS McDonnell Douglas Research Laboratories McDonnell Douglas Corporation P.O. Box 516 St. Louis, MO 63166		10. PROGRAM ELEMENT, PROJECT, TASK AREA & WORK UNIT NUMBERS 61102F, 2306, A1
11. CONTROLLING OFFICE NAME AND ADDRESS Air Force Office of Scientific Research Building 410 Bolling AFB, DC 20332		12. REPORT DATE September 1984
		13. NUMBER OF PAGES 44
14. MONITORING AGENCY NAME & ADDRESS (if different from Controlling Office)		15. SECURITY CLASS. (of this report) Unclassified
		15a. DECLASSIFICATION/DOWNGRADING SCHEDULE

16. DISTRIBUTION STATEMENT (of this Report)

Approved for public release; distribution unlimited.

17. DISTRIBUTION STATEMENT (of the abstract entered in Block 20, if different from Report)

18. SUPPLEMENTARY NOTES

19. KEY WORDS (Continue on reverse side if necessary and identify by block number)

Aluminum alloys	Powder metallurgy	Rapid solidification	Consolidation
Hot pressing	Extrusion	Explosive consolidation	Iron
Densification	Interparticle bonding	Recovery	Cerium
Microstructure	Porosity	Lithium	X Ray Diffraction
Zirconium	Degassing	Recrystallization	Electron Microscopy

20. ABSTRACT (Continue on reverse side if necessary and identify by block number)

The influence of metallurgical and process variables on the consolidation, densification, and properties of rapidly solidified aluminum alloy powders is being investigated. Cold compaction, hot pressing, powder extrusion, and explosive consolidation are being used to consolidate rapidly solidified 99.9% aluminum powder (reference material), Al-3Li-1Cu-1Mg-0.2Zr (a representative low-density, high-modulus alloy), and Al-8Fe-7Ce alloys (representative of high-temperature Al alloys). The alloys included in the study provide wide

DD FORM 1 JAN 73 1473 EDITION OF 1 NOV 65 IS OBSOLETE

UNCLASSIFIED

SECURITY CLASSIFICATION OF THIS PAGE (When Data Entered)

variations in hardness, flow stress, work hardening rate, plasticity, and oxide-film thickness. The consolidation techniques selected for the study provide variations in pressure, compaction rate, and extent of oxide-film breakdown.

Three 35-kg lots of rapidly solidified 99.9% Al, Al-3Li-1Cu-1Mg-0.2Zr, and Al-8Fe-7Ce alloy powders were prepared by vacuum atomization; and the powders were characterized with respect to particle size distribution, cooling rates, constituent phases, and volatile contaminants.

The pressure dependence of densification during cold compaction was correlated with the yield stress and work hardening of the three alloys. Complete densification with sound interparticle bonding was observed in 99.9% Al powders hot pressed at 400°C. The hot-pressed Al-Li and Al-Fe-Ce alloys contained 1-2% porosity and had weak interparticle bonding. The extrusion rate dependences of flow stress and interparticle bonding were determined for 99.9% Al and Al-Li alloy powder compacts. The rate sensitivity of flow stress for Al and Al-Li alloys was ≈ 0.2 at extrusion rates of 0.04-0.6 cm/s. Extrusions of Al at > 0.04 cm/s resulted in fully densified compacts with sound interparticle bonding and recrystallized elongated grain microstructure. The Al-Li alloy extruded at > 0.08 cm/s showed sound interparticle bonding and recovered subgrain microstructure.

Oxygen content of applied Al powder should be included. → footp.

With the objective of extending the analyses to include high strain rate effects during explosive loading, powder packs have been prepared for explosive consolidation.

The ongoing studies include the temperature, pressure, and time dependence of densification and mechanical integrity of powder compacts hot pressed at 300-500°C and 150-1000 MPa pressures; temperature and extrusion rate dependence of flow stress, microstructural evolution, and mechanical properties of alloys extruded at 400-500°C with extrusion ratios of 10:1, 20:1, and 30:1, and pressure dependence of densification and interparticle bonding in explosively consolidated alloys. The densification, interparticle bonding, microhardness, oxide-breakup and distribution, recovery and recrystallization, and mechanical properties of the consolidated products will be determined during the next reporting period.

CONTENTS

	Page
1. INTRODUCTION	1
2. RESEARCH OBJECTIVES AND APPROACH	3
3. SUMMARY OF RESULTS	4
3.1 Alloy Preparation	4
3.2 Powder Characterization	5
3.3 Consolidation of Aluminum Alloy Powders	12
3.3.1 Cold Compaction	12
3.3.2 High-Temperature Consolidation	23
3.3.3 Powder Extrusion	24
3.3.4 Explosive Compaction of Aluminum Alloys	28
4. PUBLICATIONS AND PRESENTATIONS RESULTING FROM AFOSR SUPPORT	35
5. LIST OF PERSONNEL	36
6. COUPLING ACTIVITIES WITH GROUPS DOING RELATED RESEARCH	37
REFERENCES	38

Accession For
NTIS GRA&I ☒
DTIC TAB ☐
Unannounced ☐
Justification
By
Distribution/
Availability Codes
Dist | Avail and/or Special
A-1

AIR FORCE OFFICE OF SCIENTIFIC RESEARCH (AFSC)
NOTICE OF TRANSMITTAL TO DTIC
This technical report has been reviewed and is approved for public release
Distribution is unlimited.
MATTHEW J. KERPER
Chief, Technical Information Division

LIST OF ILLUSTRATIONS

Figure | Page

1. Vacuum atomization apparatus 4
2. Particle size distributions of aluminum, Al-3Li-1Cu-1Mg-0.2Zr, and Al-8Fe-7Ce powders 6
3. Scanning electron micrographs of rapidly solidified (a) 99.9% Al, (b) Al-3Li-1Cu-1Mg-0.2Zr, (c) Al-8Fe-7Ce, and (d) Al-8Fe-4Ce powders 7
4. X-ray diffraction peaks of (a) aluminum, (b, c, and d) Al-3Li-1Cu-1Mg-0.2Zr alloy, (b) rapidly solidified, (c) annealed at 400°C for 2 h, and (d) annealed at 500°C for 2 h 9
5. X-ray diffraction peaks of (a) aluminum, (b, c, and d) Al-8Fe-4Ce alloy, (b) rapidly solidified, (c) annealed at 400°C for 2 h, and (d) annealed at 500°C for 2 h 10
6. X-ray diffraction peaks of (a) aluminum, (b, c, and d) Al-8Fe-7Ce alloy, (b) rapidly solidified, (c) annealed at 400°C for 2 h, and (d) annealed at 500°C for 2 h 11
7. Ion intensity as a function of temperature for aluminum, Al-3Li-1Cu-1Mg-0.2Zr, Al-8Fe-7Ce, and Al-8Fe-4Ce alloy powders. (Data obtained by mass spectroscopic analysis.) 13
8. Variation with compaction pressure of (a) density and (b) rate of density change with pressure ($d\rho/dp$) for aluminum, Al-3Li-1Cu-1Mg-0.2Zr, Al-8Fe-4Ce, and Al-8Fe-7Ce powders consolidated by uniaxial pressing at 25°C 15
9. Effect of powder-size distribution of (a) densification and (b) rate of density change with pressure ($d\rho/dp$) of aluminum powders consolidated by uniaxial pressing at 25°C 16
10. Effect of ram-displacement rate on densification of aluminum-powder compacts consolidated by uniaxial pressing at 25°C 16
11. Variation of density with compaction pressure for (a) aluminum and (b) Al-3Li-1Cu-1Mg-0.2Zr alloy powders consolidated by uniaxial pressing at 25°C 18
12. Variation of (a) density with effective stress and (b) density with the ratio of effective stress to yield stress of aluminum and Al-3Li-1Cu-1Mg-0.2Zr 19
13. Scanning electron micrographs of aluminum-powder compacts consolidated by uniaxial pressing at 25°C 19
14. Scanning electron micrographs of aluminum-powder compacts (with < 38-μm-diam powders) consolidated by uniaxial pressing at 25°C 20

LIST OF ILLUSTRATIONS

Figure | Page

15. Scanning electron micrographs of aluminum-powder compacts (with 125- to 180-μm-diam powders) consolidated by uniaxial pressing at 25°C..... 20

16. Scanning electron micrographs of Al-3Li-1Cu-1Mg-0.2Zr alloy powder compacts consolidated by uniaxial pressing at 25°C..... 21

17. Scanning electron micrographs of Al-8Fe-7Ce alloy powder compacts consolidated by uniaxial pressing at 25°C..... 21

18. High-magnification electron micrographs of (a) aluminum, (b) Al-3Li-1Cu-1Mg-0.2Zr, and (c) Al-8Fe-7Ce powder compacts consolidated by uniaxial pressing at 25°C..... 22

19. Optical micrographs of aluminum powder compacts consolidated by uniaxial pressing at 400°C..... 25

20. Optical micrographs of Al-3Li-1Cu-1Mg-0.2Zr alloy powder compacts consolidated by uniaxial pressing at 400°C..... 25

21. Optical micrographs of Al-8Fe-7Ce alloy powder compacts consolidated by uniaxial pressing at 400°C..... 26

22. High-magnification scanning electron micrographs of (a) Al-3Li-1Cu-1Mg-0.2Zr and (b) Al-8Fe-7Ce alloy powder compacts consolidated by uniaxial pressing at 400°C..... 27

23. Variation of flow stress with extrusion rate of aluminum and Al-3Li-1Cu-1Mg-0.2Zr powders extruded at 400°C..... 27

24. Optical micrographs of aluminum powder compacts extruded at 400°C at extrusion rates of (a) 0.01 cm/s, (b) 0.04 cm/s, (c) 0.08 cm/s, and (d) 0.16 cm/s..... 29

25. Optical micrographs of Al-3Li-1Cu-1Mg-0.2Zr alloy powder compacts extruded at 400°C at extrusion rates of (a) 0.02 cm/s and (b) 0.08 cm/s..... 31

26. Transmission electron micrographs of (a) aluminum and (b) Al-3Li-1Cu-1Mg-0.2Zr powder compacts extruded at 400°C at an extrusion rate of 0.08 cm/s..... 32

27. High-energy-rate consolidation of rapid solidification processed (RSP) alloys..... 33

LIST OF TABLES

Table		Page
1	Nominal composition and chemical analyses of the materials studied	5
2	Indentation dimensions and microhardness values of powders studied	8
3	Interplanar spacing (d) of phases detected in Al-8Fe-7Ce alloy annealed at 500°C for 2 h	12
4	Tap densities and theoretical densities of materials studied	14

1. INTRODUCTION

Rapid solidification processing (RSP) through its ability to refine microstructures and increase solid solubilities has made the development of new Al-alloy systems possible.[1-5] These alloy systems include the low-density, high-modulus, precipitation-hardenable Al-Li alloys,[1,2] high-temperature dispersion-strengthened Al-Fe-Ce alloys,[3] high-strength Al-Zn-Mg alloys,[4] and SiC whisker-reinforced aluminum alloys.[5]

The overall RSP sequence involves the rapid solidification of alloys into powder by atomization or into flakes by splat quenching followed by consolidation of the particulates into fully dense alloys. Consolidation steps include cold compaction of the particulates to about 70% of the theoretical density, vacuum hot pressing to fully densify the cold compacts, and extrusion or forging. The most important consideration for realizing the full benefits of rapidly solidified aluminum powders is optimization of the powder consolidation parameters. The powder size and shape, temperature, strain, strain rate, and type of deformation during consolidation determine the extent of densification, substructure formation, recovery and recrystallization, second-phase precipitation or resolution, and texture development. These metallurgical changes determine the microstructures and properties that can be achieved by post-consolidation thermomechanical processing and heat treatment. The most important consolidation-related microstructural features that deleteriously affect the mechanical properties of a consolidate are: (1) particle delamination as a result of improper breakdown of oxide film and poor interparticle bonding, (2) hydrogen blistering resulting from improper degassing or moisture pickup during powder preparation and consolidation, and (3) directionality in properties resulting from crystallographic texture development during consolidation. Each of these features is influenced by the type of powder consolidation.

Despite the overwhelming importance of aluminum powder compaction, especially in the case of rapidly solidified aluminum alloy powders, no systematic study has been made of the interrelationship between powder and process variables and the resultant microstructures and mechanical properties of compacts. The present investigation is a systematic study of the influence of metallurgical and process variables on the consolidation, densification, and proper-

ties of rapidly solidified aluminum alloy powders. Aluminum (99.9% pure reference material), a representative low-density high-modulus Al-Li alloy, and a representative high-temperature dispersion-strengthened Al-Fe-Ce alloy were selected to determine the effects of metallurgical parameters on consolidation. The selected alloys have wide variations in hardness, flow stress, work hardening rate, plasticity, and oxide-film thickness. Vacuum hot pressing, hot isostatic pressing, powder extrusion, and explosive compaction have been selected for evaluating consolidation process parameters. The consolidation techniques selected for the study provide variations in pressure, compaction rate, and extent of oxide-film breakdown.

The goal of the program is to construct consolidation diagrams in a manner analogous to superplastic forming and sintering diagrams. Such generalized relations and consolidation diagrams can then be used to optimize consolidation variables, obtain beneficial combinations of properties in products processed from rapidly solidified powders, and provide guidelines for consolidation and near-net-shape processing of aluminum powders.

2. RESEARCH OBJECTIVES AND APPROACH

The overall objectives of this program are to (1) determine the effects of powder shape, size, size distribution, surface-oxide film, entrapped hydrogen, and powder plastic-flow characteristics on densification, interparticle bonding, microstructure, and texture development during consolidation by hot pressing, extrusion, and dynamic compaction; (2) determine the effects of consolidation process variables (temperature, pressure, and compaction rate) on the microstructures and mechanical properties of aluminum powder compacts; and (3) establish generalized relations between material and process variables and construct consolidation diagrams to provide guidelines for selecting and optimizing aluminum consolidation schedules.

The specific objectives of the first year of the research program, which is reported here, were to:

(a) prepare rapidly solidified 99.9% pure aluminum, Al-Li-Cu-Mg-Zr, and Al-Fe-Ce alloy powders;

(b) determine powder size distributions, solidification rates from dendrite spacing measurements, microhardness, oxide-film thickness, and hydrogen concentrations;

(c) determine yield stress, work hardening rate, and ductilities of the alloys from tensile property measurements on specimens prepared from cast, forged, and rolled alloy sheets;

(d) determine tap densities and cold compacted densities of the powders; and

(e) evaluate the effects of powder parameters on the densification during cold compaction.

3. SUMMARY OF RESULTS

3.1 Alloy Preparation

Three 35-kg lots of rapidly solidified 99.9% Al, Al-3Li-1Cu-1Mg-0.2Zr, and Al-8Fe-7Ce alloy powders were prepared by vacuum atomization at Homogeneous Metals, Inc., Clayville, NY, using the apparatus shown in Figure 1. Each alloy was induction melted in an argon-filled pressure chamber. Once the melt had been homogenized and heated to the desired temperature, the sealing door was opened and the melt ejected through a transfer tube into the evacuated powder collection chamber. The melt was atomized and solidified by the escape of the pressurizing gas; it cascaded into a vessel which could be valved off from the chamber for further handling.

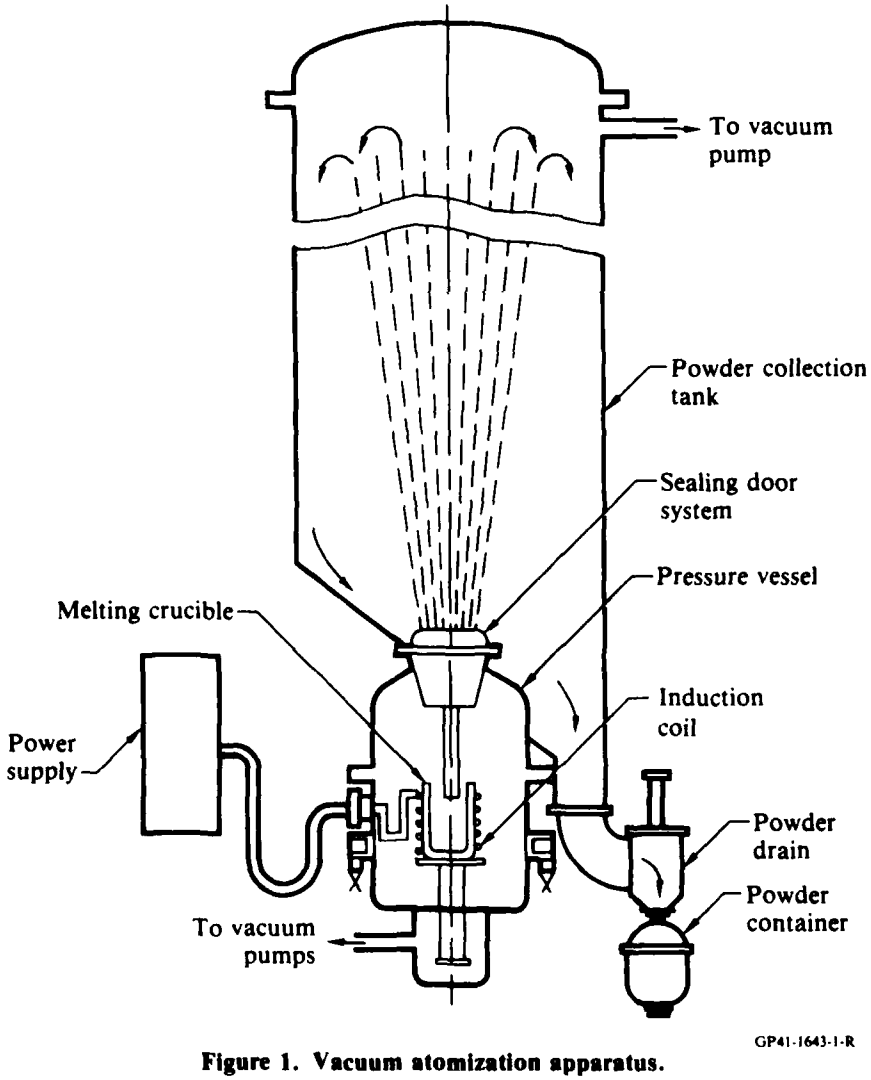

Figure 1. Vacuum atomization apparatus.

In addition to the above alloys, one kg of Al-8Fe-4Ce alloy powder prepared by air atomization at Alcoa Technical Center, PA, was procured from Air Force Materials Laboratory, AFWAL.

The nominal compositions and chemical analyses of the alloys are listed in Table 1.

3.2 Powder Characterization

Particle-size distributions of the as-solidified powders were obtained by sieving ≈ 20 g samples according to ASTM E161-70 using electroformed sieves. Because of the more precise tolerances and freedom from clogging and particle entrapment, the electroformed sieves produce particle-size distribution data superior to those obtainable using wire-woven sieves. Typical particle-size distributions by weight, plotted on probability paper, are shown in Figure 2 for different alloys. The weight-frequency plots show near log normal distributions of particle sizes for all three metals. The geometric mean sizes are 66 μm for aluminum and 94 μm for Al-3Li-1Cu-1Mg-0.2Zr and Al-8Fe-7Ce alloys. In all three alloys 80% of the particles are between 30 and 150 μm. This distribution is ideal because the size range assures efficient tap density and microstructural uniformity in consolidated forms. Furthermore, excessive oxide formation and explosion hazard are minimized because of the absence of ultrafine particles.

The cooling rates of the powders were determined from dendrite-arm-spacing measurements. For the size ranges of 30-150 μm, the cooling rates were 10^4-10^3 K/s.

Table 1. Nominal compositions and chemical analyses of the materials studied.

Nominal compositions	Actual compositions
Al	99.9% Al
Al-3Li-1Cu-1Mg-0.2Zr	Al-2.92Li-1.0Cu-1.2Mg-0.22Zr
Al-8Fe-7Ce	Al-8.6Fe-7.19Ce
Al-8Fe-4Ce	ND

GP41-1643-30-R

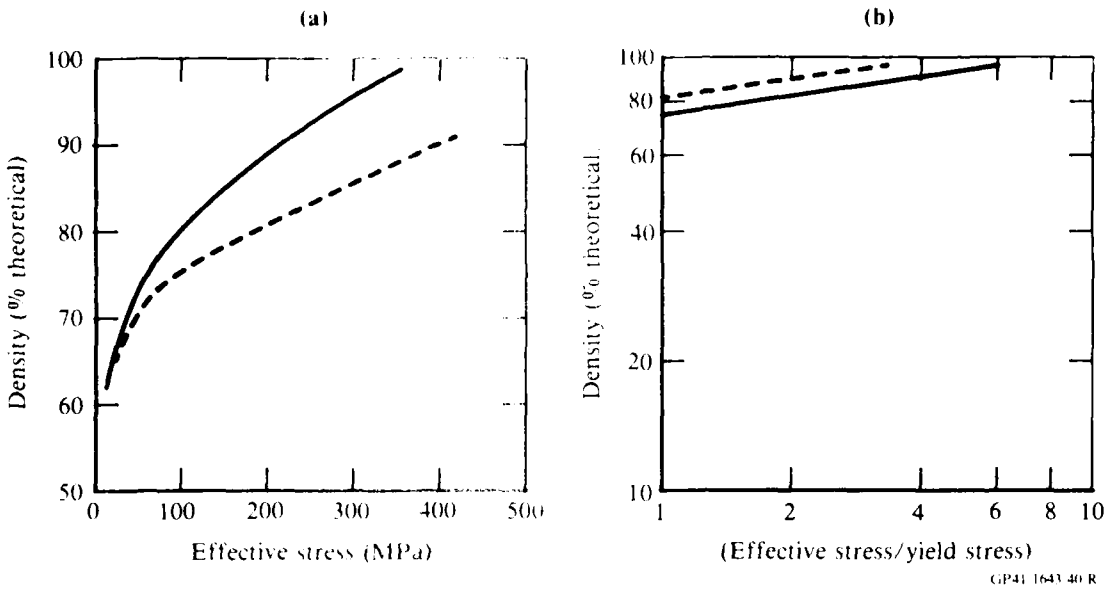

Figure 12. Variation of (a) density with effective stress and (b) density with the ratio of effective stress to yield stress of (——) aluminum and (- - -) Al-3Li-1Cu-1Mg-0.2Zr.

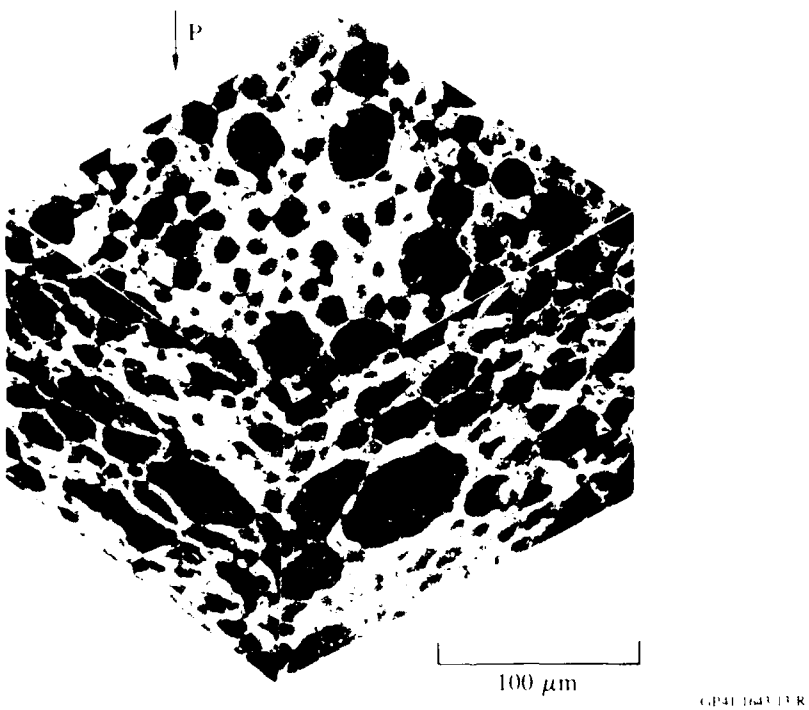

Figure 13. Scanning electron micrographs of aluminum-powder compacts consolidated by uniaxial pressing at 25 °C.

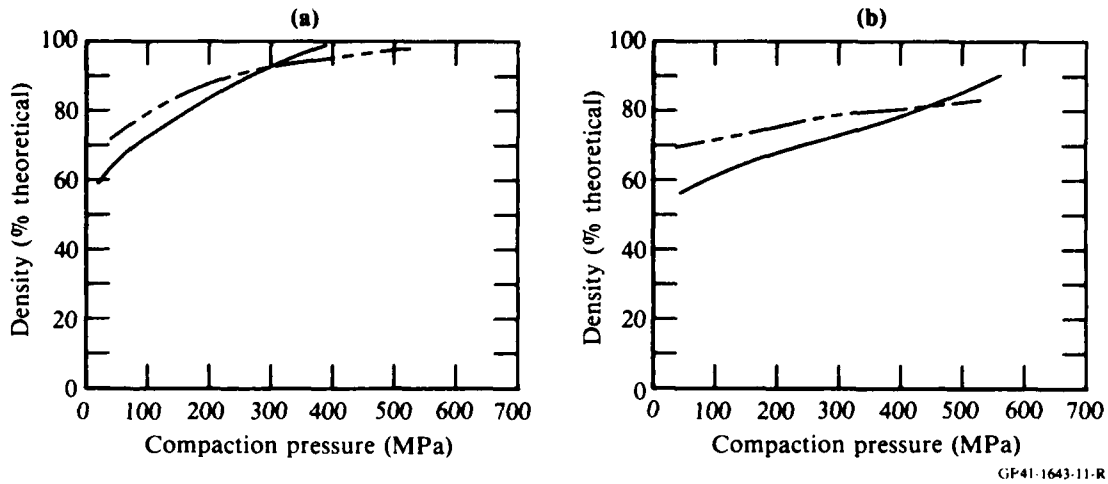

Figure 11. Variation of density with compaction pressure for (a) aluminum and (b) Al-3Li-1Cu-1Mg-0.2Zr alloy powders consolidated by uniaxial pressing at 25°C: (— — — —) experimental values and (————) calculated from Equation (4).

(4) should be replaced by an effective stress σ_{eff} which is the applied load divided by the contact area projected in a plane normal to the applied load, which is a fraction of the cylindrical die face area.

Figure 12 shows plots of $\ln\rho$ as a function of $\ln(\sigma_{eff}/Y)$ for Al and Al-3Li-1Cu-1Mg-0.2Zr. Based on the microhardness values of the powders and available tensile data for solution-annealed alloys, yield stress values of 56 and 224 MPa were assumed for Al and Al-3Li-1Cu-1Mg-0.2Zr, respectively. The densification curves shown in Figures 12a and 12b follow the same trend observed for the plastic deformation of Al and Al-3Li-1Cu-1Mg-0.2Zr.

Microstructures of aluminum powder compacts are shown in Figures 13-18. In aluminum powder compacts significant plastic deformation (> 50% plastic strain) of powder particles is observed. Close to 99% of theoretical density could be obtained by cold compacting Al powder. The apparent lack of interparticle bonding in Figure 13 is due to heavy etching of the compact for scanning electron microscopic examination. The Al-3Li-1Cu-1Mg-0.2Zr alloy shows a larger number of voids and less plastic deformation than in Al. In agreement with the high work-hardening exponent observed, Al-8Fe-7Ce exhibits the lowest density (≈ 96% of theoretical density) and the least amount of plastic deformation.

Transitional restacking is followed by a compaction stage in which particles deform plastically to fill the voids in the powder. The pressure dependence of densification during this stage of compaction has been described by an empirical relation[7]

$$\ln\left(\frac{1}{1-\rho}\right) = k_1 P + k_2 , \tag{1}$$

where ρ is the fraction of theoretical density of the powder, P is the compaction pressure, and k_1 and k_2 are constants. The constant k_1 is related to the yield strength σ_y of the constituent powder particles by the relation

$$k_1 = \frac{1}{3\sigma_Y} , \tag{2}$$

and k_2 is related to the powder size, morphology, and the degree of densification achieved during transitional restacking by the expression

$$k_2 = \ln\left(\frac{1}{1-\rho_o}\right) + B . \tag{3}$$

In Equation (3), ρ_o is the relative density after transitional restacking, and B is a constant which decreases with decreasing particle size and increasing sphericity (B = 0 for spherical particles). Combining Equations (1), (2), and (3),

$$\ln(1-\rho) = [\ln(1-\rho_o) - B] - (P/3\sigma_Y) . \tag{4}$$

The density increases with increasing pressure, increasing relative density after transitional restacking, increasing values of B, and decreasing yield strength of the particle material.

The pressure dependence of densification calculated from Equation (4) is compared with experimentally determined values for Al and Al-Li-Cu-Mg-Zr alloys in Figure 11. The equation does not correctly predict the pressure dependence of densification because work hardening of the powder particles is included in the above treatment.

An accurate description of pressure dependence of densification should take into account the porosity of the compact, and the pressure P in Equation

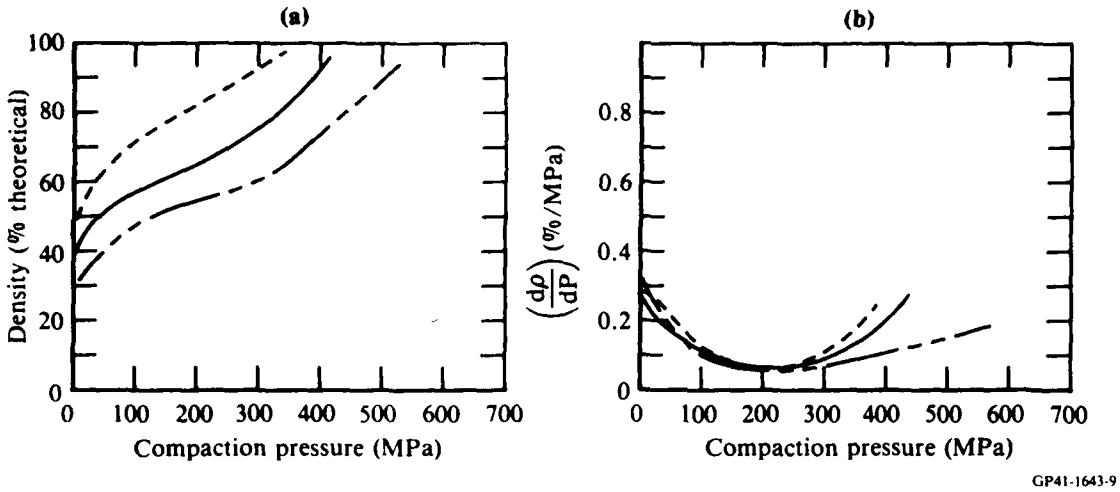

Figure 9. Effect of powder-size distribution on (a) densification and (b) rate of density change with pressure $\left(\frac{d\rho}{dP}\right)$ of aluminum powders consolidated by uniaxial pressing at 25°C. Powder size ranges: (– – – – –) 10-260 μm, (————) < 38 μm, and (— – – —) 125-180 μm.

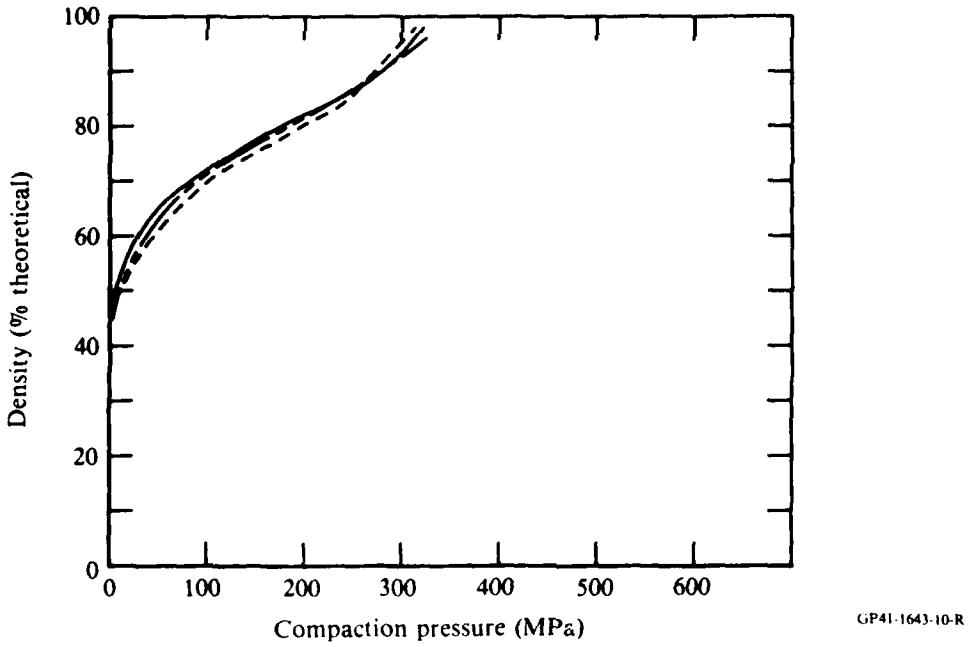

Figure 10. Effect of ram-displacement rate on densification of aluminum-powder compacts consolidated by uniaxial pressing at 25°C. Initial powder compact height is 1.75 cm, final powder compact height is 0.75 cm. Ram displacement rates: (— – – —) 2.5×10^{-3} cm/s^{-1}, (– – – – –) 5.0×10^{-3} cm/s, and (————) 1.0×10^{-2} cm/s.

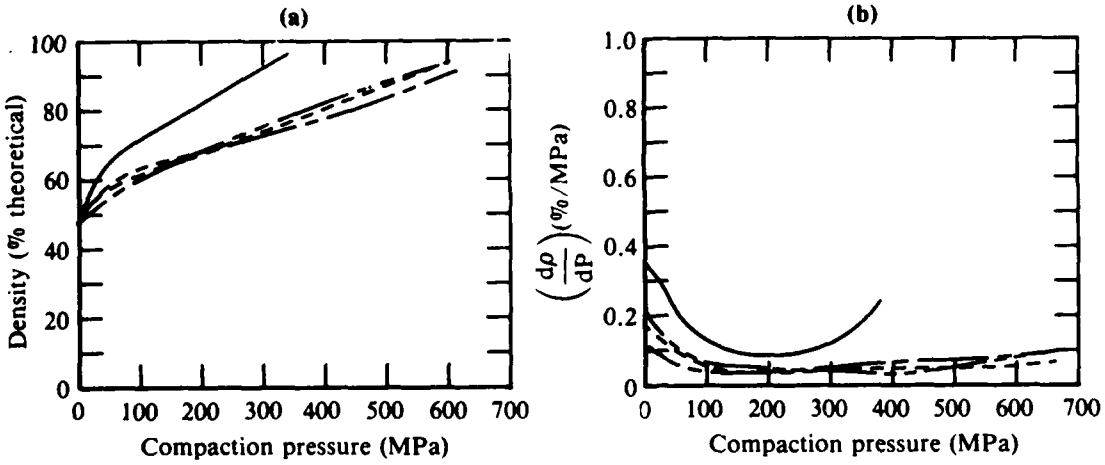

Figure 8. Variation with compaction pressure of (a) density and (b) rate of density change with pressure $\left(\frac{d\rho}{dP}\right)$ for (————) aluminum, (- - - - -) Al-3Li-1Cu-1Mg-0.2Zr, (—— - ——) Al-8Fe-4Ce, and (—— - - ——) Al-8Fe-7Ce powders consolidated by uniaxial pressing at 25°C.

ductility. The pressure required for complete densification is lower, the transitional restacking stage is longer, and the rate of density change with pressure is higher for aluminum than for the alloys.

In the transitional restacking stage of compaction, powder consolidation occurs by the movement of powder particles past one another and repacking. The amount of particle repacking that occurs during the transitional restacking stage further depends on the size and shape distributions of particles and the rate of pressure application. The effect of particle-size distribution on densification is shown in Figure 9, which indicates that powders with normal distributions and large standard deviations from the mean size (curve A in Figure 9a) can pack more closely than powders having a small standard deviation (curves B and C in Figure 9a) because of the ease with which small particles orient themselves into the interstices of groups of larger particles. The densification curves in Figure 10 indicate that the rates of pressure application have no significant effect on densification. However, very high rates of pressure application can cause premature immobilization of particles because high compressive stresses on the particles tend to block open passages.

mass. Tap-densities are listed in Table 4. The smaller oxide thickness of pure aluminum particles results in high friction between particles and reduces interparticle sliding, which accounts for the low tap density of the aluminum powders. The Al-Li-Cu-Mg and Al-Fe-Ce alloys with thicker oxide films have reduced interparticle friction, increased interparticle sliding, and higher tap density.

Cold compaction experiments were performed to determine the effects of pressure on bulk movement of particles as well as the deformation and fracture of particles, the two basic processes that contribute to densification during compaction. The powders were packed in a 12.5-mm-diameter cylindrical die and compacted in a 250-kN hydraulic load frame. The ratio of the height to the diameter of the powder compact was maintained at < 0.5 to insure uniform densification. The ram displacement as a function of applied load was monitored and the linear displacement of the ram was used to calculate the density of the compact assuming constancy of mass of the alloy and cross-sectional area of the compaction die.

Densification of powder particles progresses in three stages during compaction as shown in Figures 8a and 8b. The first stage, in which density increases rapidly with pressure, involves the bulk movement of particles, usually referred to as transitional restacking. This stage is followed by a second in which the rate of change of density with pressure is constant. This second stage is dominated by the plastic deformation of the particles. The final stage of densification involves particle fragmentation and interparticle bonding. This last state is more pronounced in aluminum because of its high

Table 4. Tap densities and theoretical densities of materials studied.

Alloy	Theoretical density (g/cm^3)	Tap density (g/cm^3)	Tap density (% theoretical density)
Al	2.7	1.41	52.0
Al-3Li-1Cu-1Mg-0.2Zr	2.484	1.6	64.4
Al-8Fe-4Ce	2.95	1.86	63.0
Al-8Fe-7Ce	2.994	2.0	66.9

GP41-1643-32-R

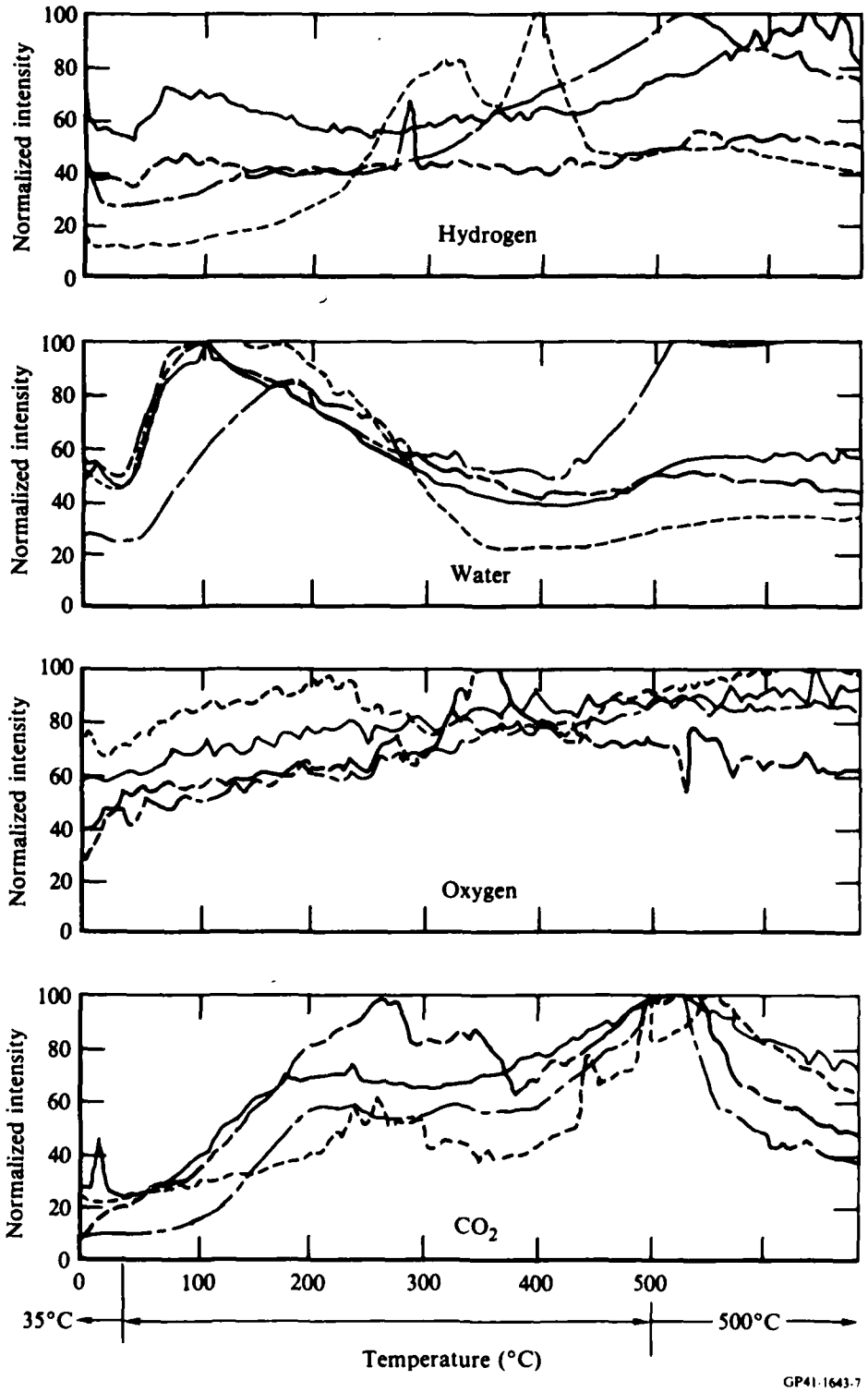

Figure 7. Ion intensity as a function of temperature for (————) aluminum (– – – – – – – – –) Al-3Li-1Cu-1Mg-0.2Zr, (————– – ————) Al-8Fe-7Ce, and (————– – –————) Al-8Fe-4Ce alloy powders. (Data obtained by mass spectroscopic analysis.)

Table 3. Interplanar spacing (d) of phases detected in Al-8Fe-7Ce alloy annealed at 500°C for 2 h.

d - spacings (nm) reported in reference	d - spacings (nm) determined in the present investigation
0.680	
0.540	0.54378
0.515	
0.445	0.44615
0.376	0.37697
0.319	0.31921
0.316	0.31699
0.300	0.30079
0.287	
0.275	
0.274	
0.260	0.26033
0.2425	0.24327
	0.23412
0.225	0.22539
0.222	0.22273
	0.20987
0.201	0.20251

GP41-1643-33-R

Figure 7 shows the ion intensity of hydrogen, water, oxygen, and carbon dioxide as a function of temperature for aluminum and the three aluminum alloys. Significant hydrogen evolution occurs at 400-500°C in aluminum and Al-8Fe-4Ce and at 350-400°C in Al-Li alloy. The hydrogen evolution is considerably less in Al-Fe-Ce alloys and occurs at a lower temperature--300°C. Almost all the water evolution occurs at 100-200°C in all the alloys. No significant differences in oxygen evolution was detected in the four alloys. Carbon dioxide evolution in all the alloys occurs at two temperature ranges--200-300°C and 500°C.

3.3 Consolidation of Aluminum Alloy Powders

3.3.1 Cold Compaction

The tap density of each alloy powder was determined by filling a 35-mm-diameter, 105-mm-long cylindrical steel container with 120 g of powder, vibrating the container for 24 h, and measuring the volume of the settled

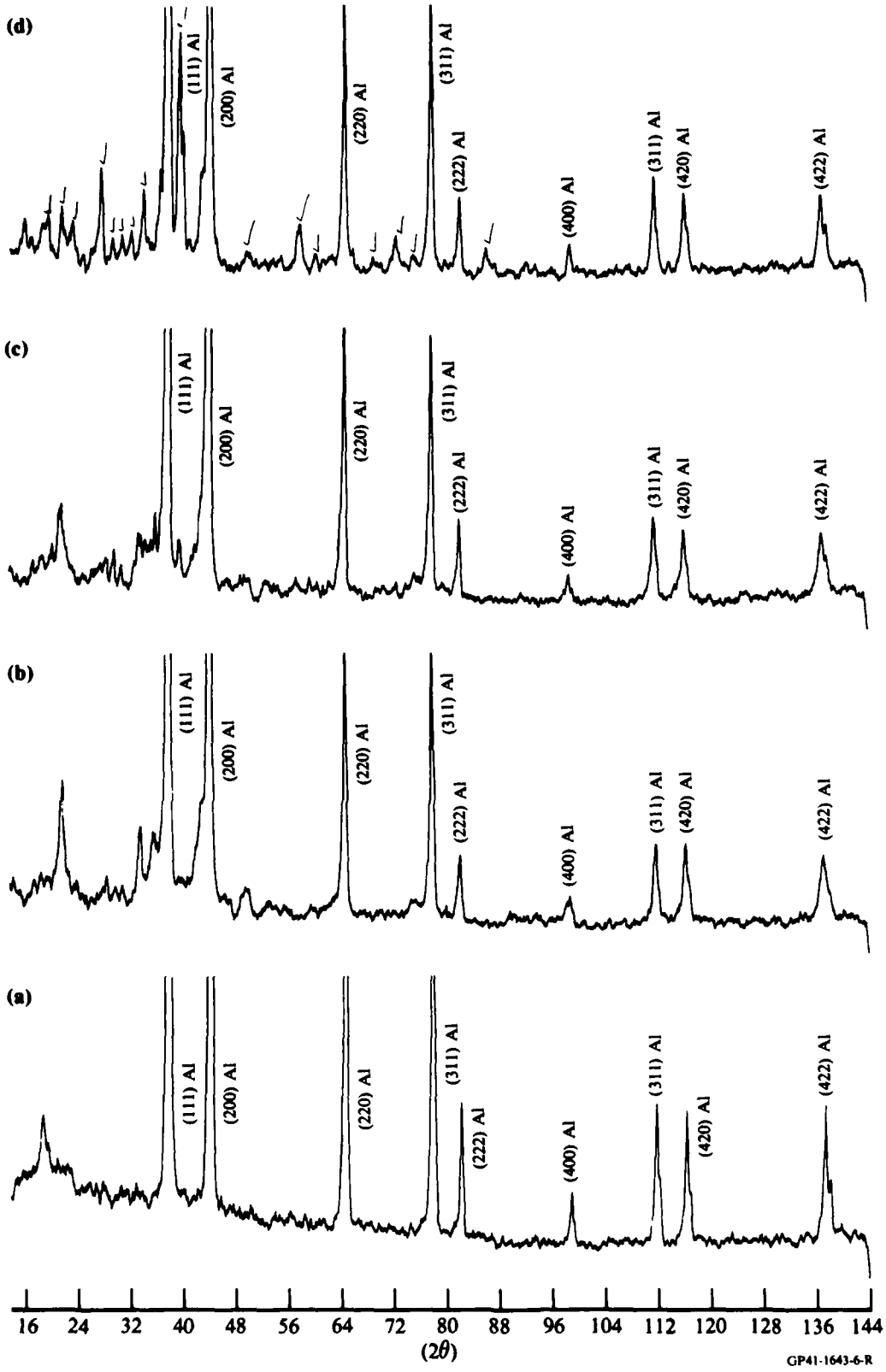

Figure 6. X-ray diffraction peaks of (a) aluminum, (b, c, and d) Al-8Fe-7Ce alloy, (b) rapidly solidified, (c) annealed at 400°C for 2 h, and (d) annealed at 500°C for 2 h.

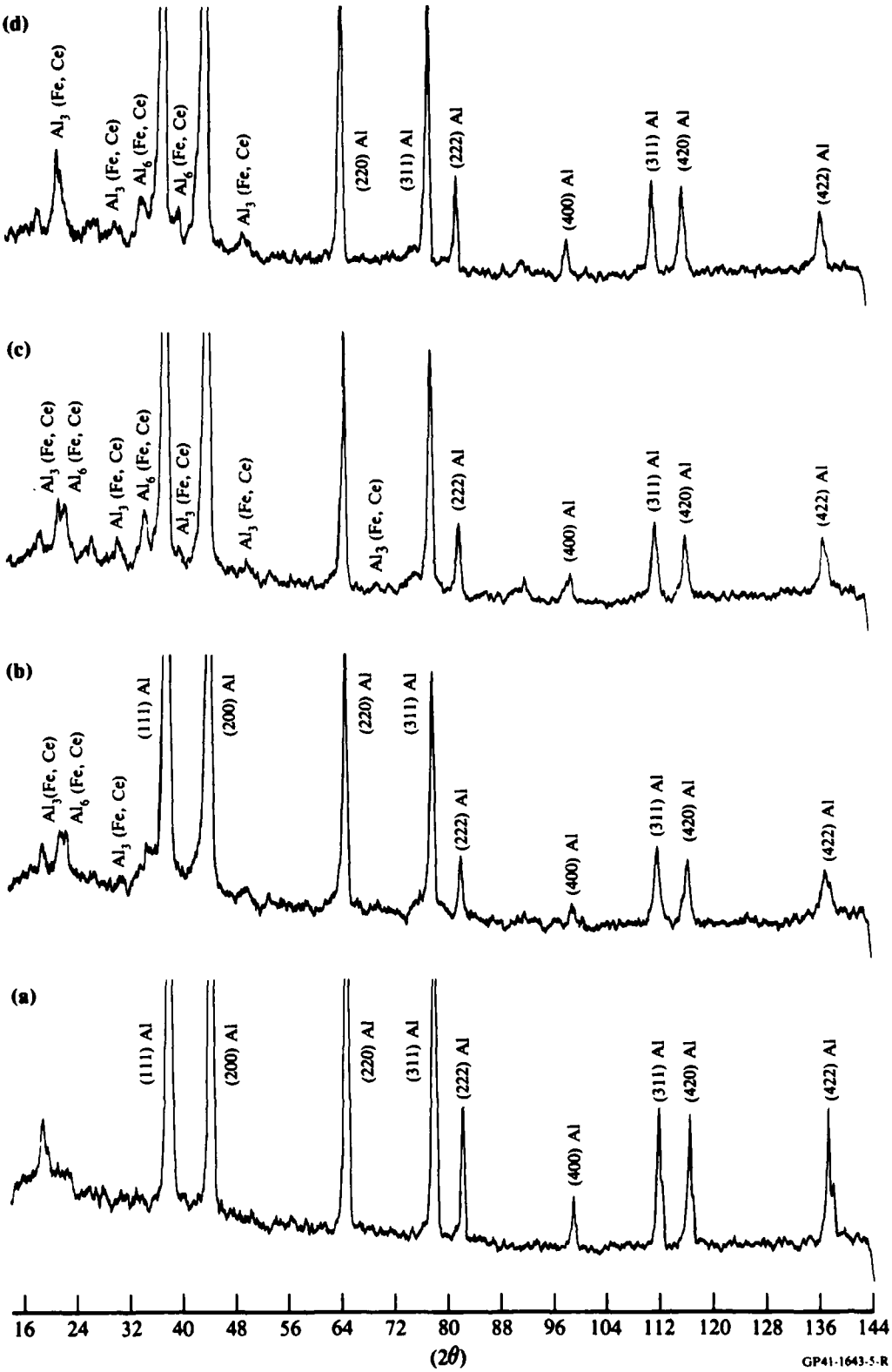

Figure 5. X-ray diffraction peaks of (a) aluminum, (b, c, and d) Al-8Fe-4Ce alloy, (b) rapidly solidified, (c) annealed at 400°C for 2 h, and (d) annealed at 500°C for 2 h.

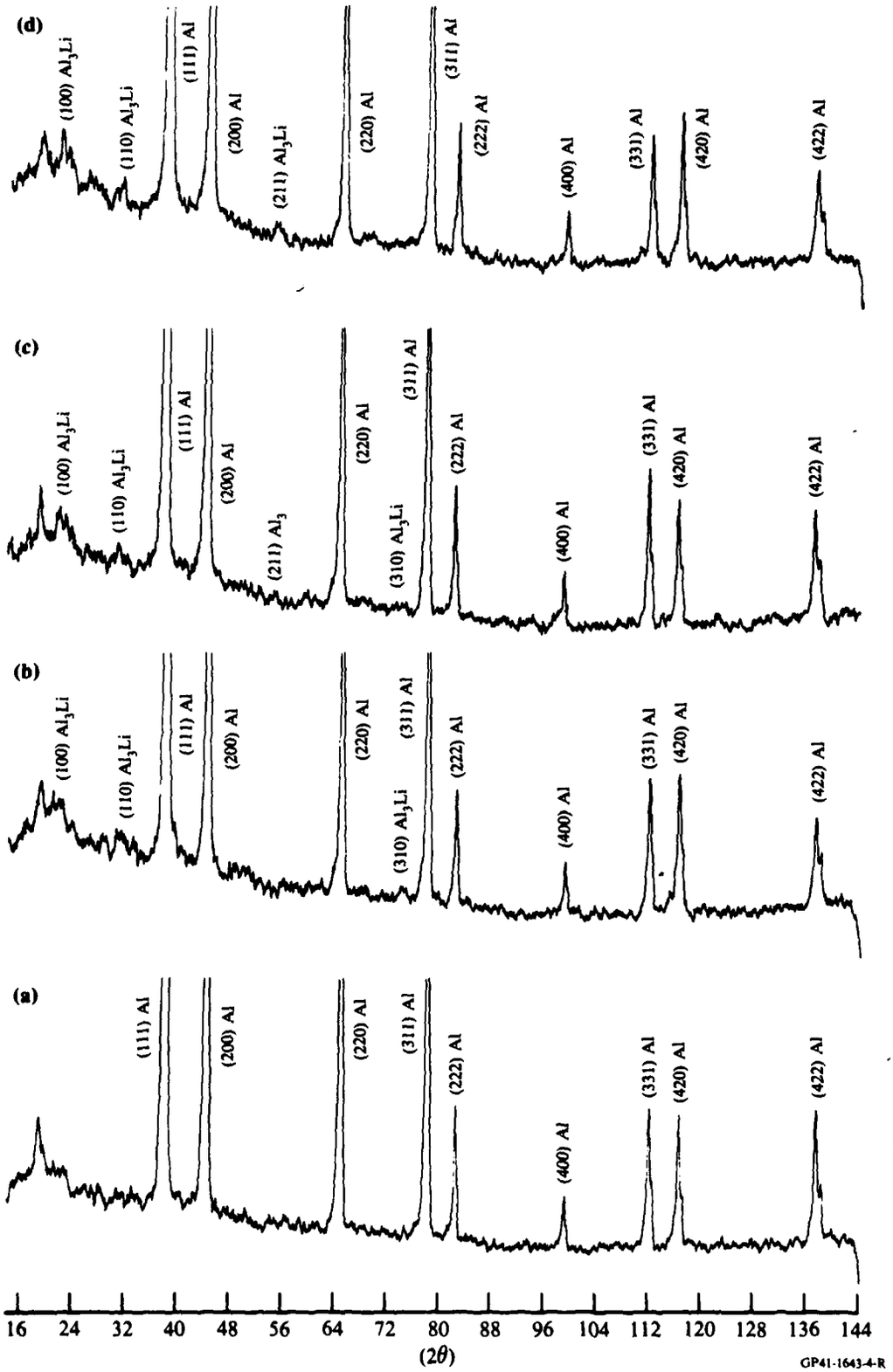

Figure 4. X-ray diffraction peaks of (a) aluminum, (b, c, and d) Al-3Li-1Cu-1Mg-0.2Zr alloy, (b) rapidly solidified, (c) annealed at 400°C for 2 h, and (d) annealed at 500°C for 2 h.

Table 2. Indentation dimensions and microhardness values of powders studied.

Alloy	Applied load (g)	Mean indentation diagonal length* (μm)	Microhardness
Al	10	27.0	25.4
Al-3Li-1Cu-Mg-0.2Zr	10	14.0	94.6
Al-8Fe-7Ce	10	13.8	97.4
Al-8Fe-4Ce	15	16.9	97.4

*Average of 10 readings

GP41-1643-31-R

The rapidly solidified Al-3Li-1Cu-1Mg-0.2Zr alloy consists of predominantly Al-Li-Cu-Mg solid solution and a small volume fraction of Al_3Li (δ') precipitates. Upon annealing at 400 and 500°C, the equilibrium AlLi and Al_6Li_3Cu (T_2) phases are formed. However, because of the small volume fraction, these phases were not detected by x-ray diffraction. Transmission electron microscopy was used instead.

In the Al-Fe-Ce alloys, a large number of intensity peaks other than those of Al were observed even in the rapidly solidified condition, indicating of phase separation during cooling. These additional peaks were more intense in the 400 and 500°C annealed alloys. In the Al-8Fe-4Ce alloys most of the additional peaks could be identified as $Al_3(Fe,Ce)$ or $Al_6(Fe,Ce)$. However, in the Al-8Fe-7Ce alloy, there were numerous peaks which could not be identified unambiguously. The interplanar spacings of the unidentified phases and the values previously reported for different phases in this system[6] are given in Table 3. Transmission electron microscopy will be used to identify these phases.

The evolution of volatile contaminants in the alloy powders was studied by mass spectroscopic analysis. Approximately 10-15 mg of alloy powder was heated from 25 to 500°C at the rate of 25-30°C per minute in the solid-sampling probe of the Vacuum Generator Model ZAB-3F mass spectrometer. The mass spectrometer was repetitively scanned over the mass range of interest as volatile materials evolved from the sample. The scan rate for the mass spectrometer was 5 s per decade of mass from 600 to 1 atomic mass units with a scan reset time of 2 s. Mass spectra so obtained were recorded with the aid of a data acquisition system and processed and analyzed after completion of a scan.

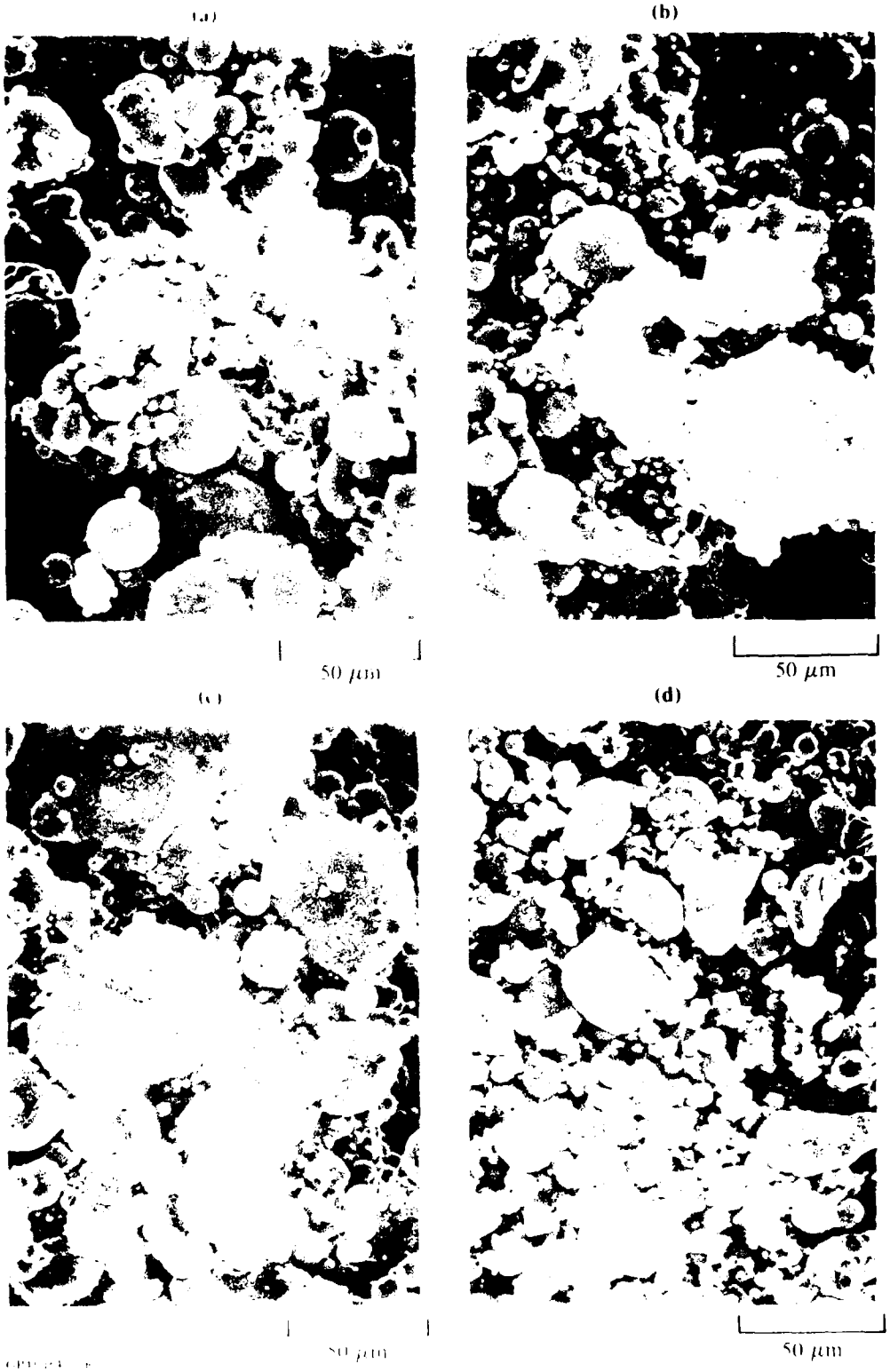

Figure 3. Scanning electron photomicrographs of rapidly solidified (a) 99.9% Al, (b) Al-[illegible]Fe-[illegible]Mg-[illegible]Zr-[illegible], (c) Al-8Fe-7Ce, and (d) Al-8Fe-4Ce powders.

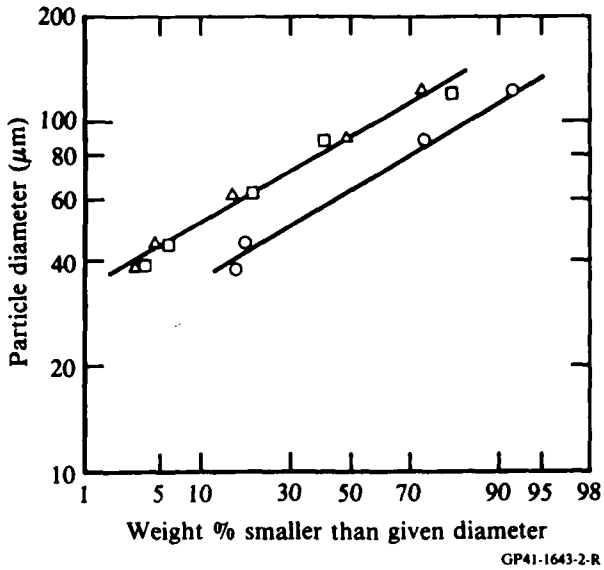

Figure 2. Particle size distributions of (○) aluminum, (△) Al-3Li-1Cu-1Mg-0.2Zr, and (□) Al-8Fe-7Ce powders.

Scanning electron micrographs of typical powders are shown in Figure 3. The particles are spherical with dendritic or cellular microstructures over the entire range of particle sizes. Powder agglomerates such as those shown in Figure 3a are more numerous in Al than in the other alloy powders. The Al-8Fe-4Ce alloy powders produced by ALCOA have a large number of irregularly shaped particles.

The rapidly solidified powders were mounted in lucite and prepared for metallographic examination, and microhardness measurements were made. The applied loads, indentation dimensions, and microhardness values are listed in Table 2. The hardness values of the Al-Li and Al-Fe-Ce alloys are about four times that of pure aluminum.

The phases present in the rapidly solidified and heat-treated samples were determined by x-ray diffractometry using monochromatic Cu K_α radiation. For high-temperature anneals, the samples were enclosed in airtight stainless steel tubes, annealed at 400 and 500°C for 2 h, and cooled to 25°C in air. Figures 4-6 show the diffracted x-ray intensity peaks for the three alloys and the aluminum standard in the rapidly solidified and heat-treated conditions.

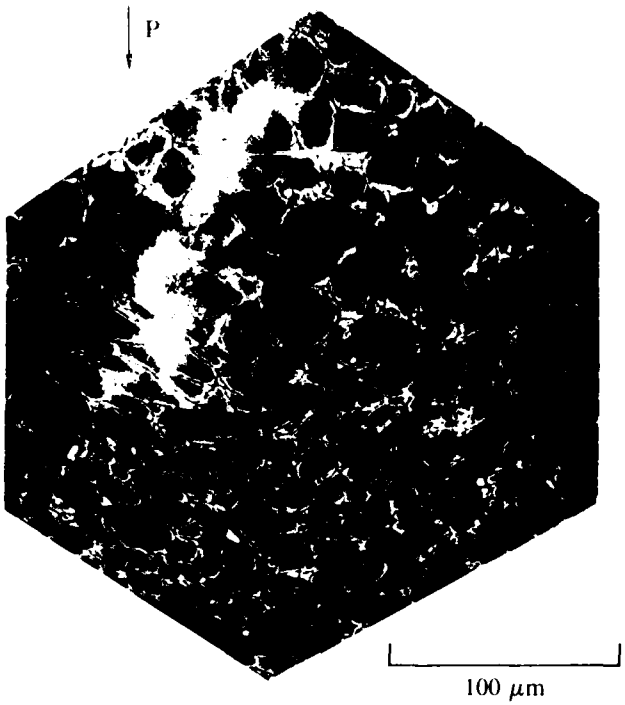

GP41-1643-14-R

Figure 14. Scanning electron micrographs of aluminum-powder compacts (with <38-μm-diam powders) consolidated by uniaxial pressing at 25°C.

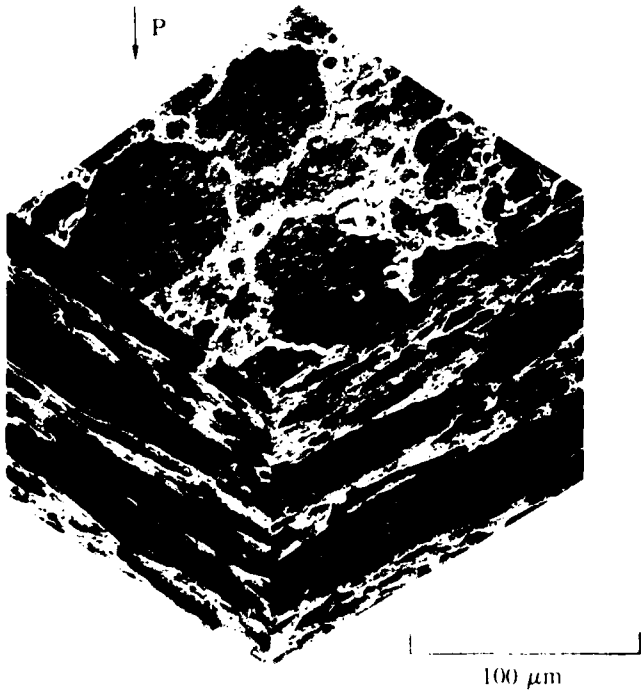

GP41-1643-15-R

Figure 15. Scanning electron micrographs of aluminum-powder compacts (with 125 to 180-μm-diam powders) consolidated by uniaxial pressing at 25°C.

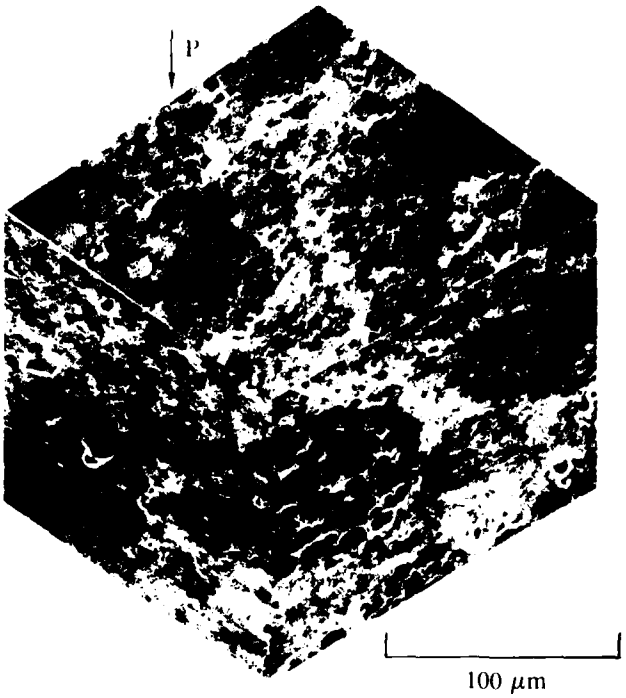

GP41-1643-16-R

Figure 16. Scanning electron micrographs of Al-3Li-1Cu-1Mg-0.2Zr alloy powder compacts consolidated by uniaxial pressing at 25°C.

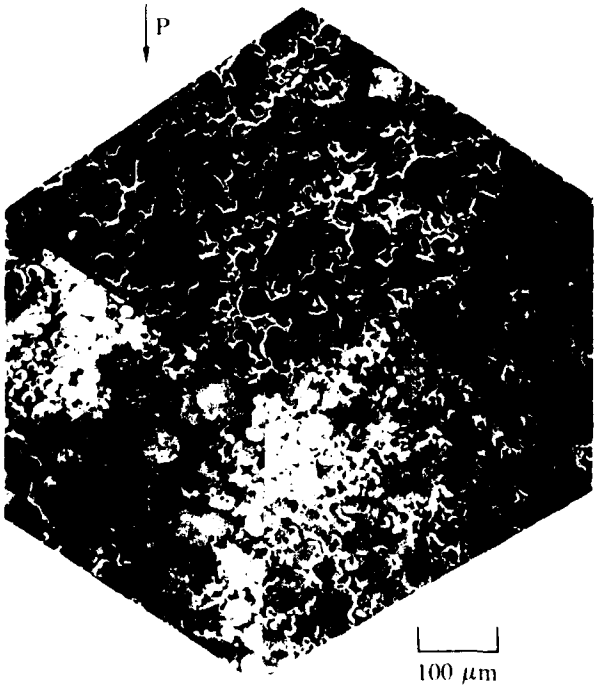

GP41-1643-17-R

Figure 17. Scanning electron micrographs of Al-8Fe-7Ce alloy powder compacts consolidated by uniaxial pressing at 25°C.

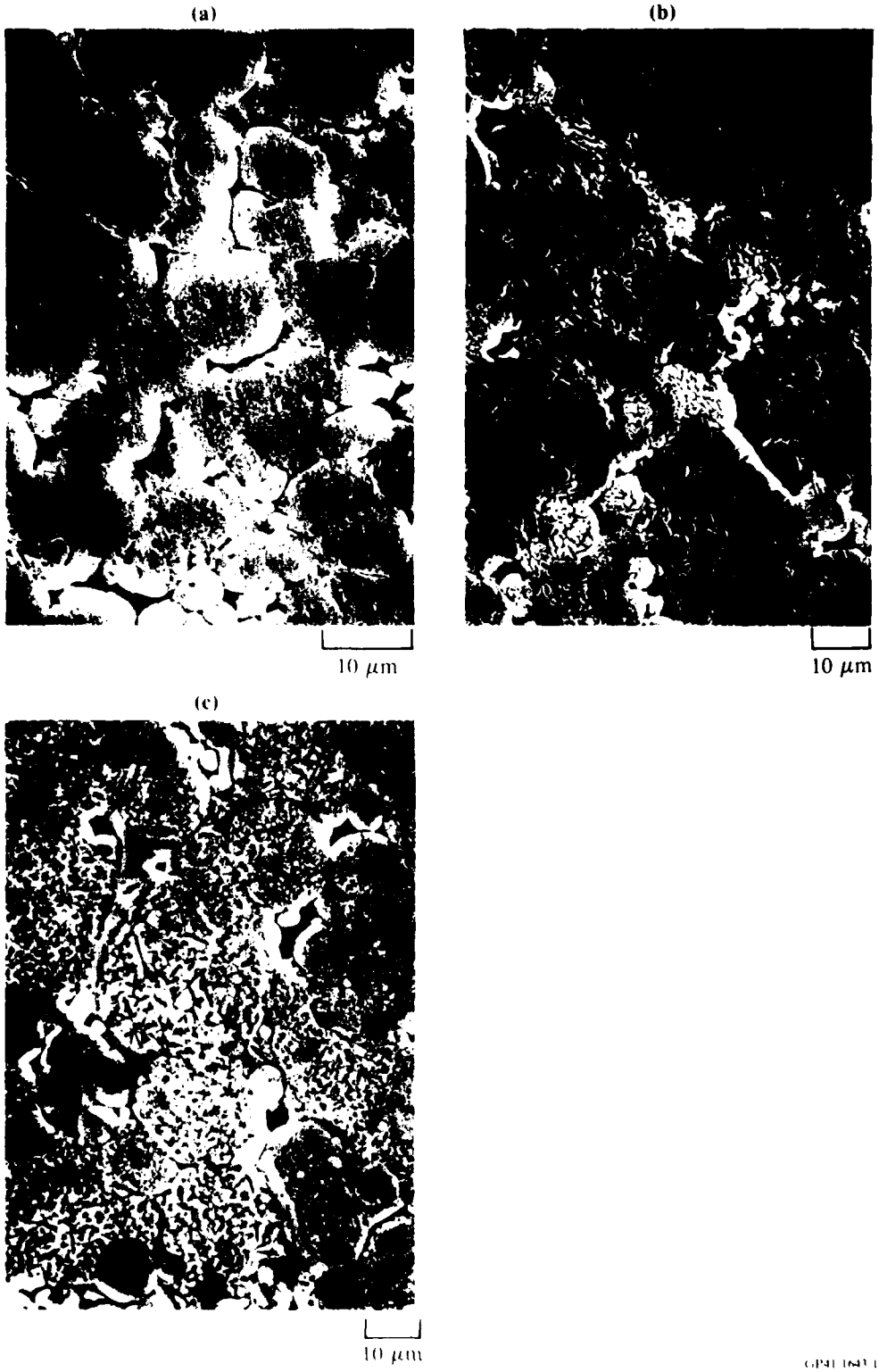

Figure 18. High-magnification electron micrographs of (a) aluminum, (b) Al-3Li-1Cu-1Mg-0.2Zr, and (c) Al-8Fe-7Ce alloy powder compacts consolidated by uniaxial pressing at 25°C.

3.3.2 High-Temperature Consolidation

Preliminary hot-pressing experiments at 400°C were performed with 12.5-mm-diameter cylindrical dies using alumina rams. The powders were first cold compacted to 90-95% of the theoretical densities. The compacts were then inserted between two platens in a furnace mounted on a hydraulic press. After the compact and the platens were heated to the desired temperature, pressure application was begun. The samples were compacted at constant pressure, and the time dependence of compaction rates was determined from the hydraulic ram displacements.

Densification during hot pressing occurs predominantly by plastic flow and increased diffusional mass transport. The available experimental data required to model aluminum powder densification during hot pressing are minimal and inconclusive. Densification by hot pressing of particulates progresses by (1) development of intimate physical contact between particles, (2) formation of metallic bonds, and (3) bond interdiffusion and recrystallization and/or grain growth across the interfaces.

Development of physical contact between particles occurs through initial removal of local asperities by interface creep under applied pressure followed by the diffusion-aided removal of micropores or voids. Creep deformation of the surface, not diffusion, is the rate-controlling mechanism for the removal of asperities by plastic deformation under pressure. Therefore, the initial stage of densification is greatly influenced by the same metallurgical and process variables that affect the high-temperature creep characteristics of the alloy. The process variables include temperature, pressure, and time; and the metallurgical variables include alloy composition, plastic flow properties of the alloy, diffusion coefficients, and grain size.

Because the individual particles undergo creep deformation during hot pressing, the flow-stress/strain-rate equations governing high-temperature creep can be used to model the hot pressing. A phenomenological expression relating the strain-rate $\dot{\varepsilon}$ to flow stress σ under steady-state conditions at high temperature can be written in the form:[8]

$$\frac{\dot{\varepsilon} kT}{DGb} = A\left(\frac{b}{d}\right)^{p}\left(\frac{\sigma}{G}\right)^{n}, \tag{5}$$

where $\dot{\varepsilon}$ = steady-state strain rate, k = Boltzmann constant, T = temperature, D = diffusion coefficient, G = shear modulus, b = Burgers vector, d = grain size, n = stress exponent, and A and p are constants. In this program, expressions for the creep rates as functions of material variables, temperature, and stress will be determined, and densification rates will be determined from creep-rate equations.

In the initial stages of hot pressing, the powder contains isolated pores and the contact area is, therefore, only a fraction of the cylindrical die face area.

From the experimentally measured contact area and applied load, the effective stress σ_{eff} can be calculated, and σ in Equation (5) can be replaced by σ_{eff}. Because surface diffusion along pore surfaces also plays a dominant role during the initial stage of densification, the surface energy γ as part of the driving force for transport must be incorporated into Equation (5). Approximating the pores to cylinders of radius r, the total driving force becomes $\sigma_{eff} = \gamma/r$.[9] The linear strain rate in Equation (5) can be converted to densification rate using constancy of mass and the cross-sectional area of the hot-press die.

The experimentally determined densification rate will be correlated with the rate predicted from creep equations.

Figures 19-22 are optical micrographs of Al, Al-3Li-1Cu-1Mg-0.2Zr, and Al-8Fe-7Ce hot pressed at 400°C. Complete densification with significant plastic deformation of powder particles occurred in Al. However, Al-Fe-Ce and Al-Li-Cu-Mg-0.2Zr alloys exhibit voids and weak interparticle bonding. Transmission electron microscopic examination and tensile property measurements of the hot-pressed compacts are in progress.

3.3.3 Powder Extrusion

Extrusion combines hot compacting and mechanical working to yield a fully dense compact. In hot pressing, little plastic flow takes place beyond that necessary for consolidation. In extrusion, however, large hydrostatic compressive forces occur, and a unidirectional force component makes the compact flow through a die with extensive plastic deformation. In particular, the frictional forces in the hot-extrusion process yield a shear component that

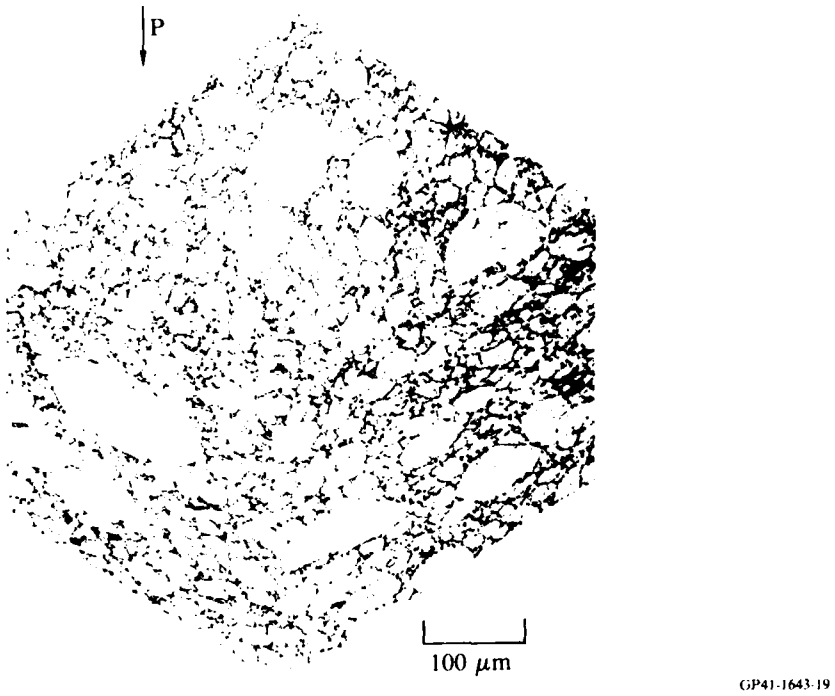

Figure 19. Optical micrographs of aluminum powder compacts consolidated by uniaxial pressing at 400 °C.

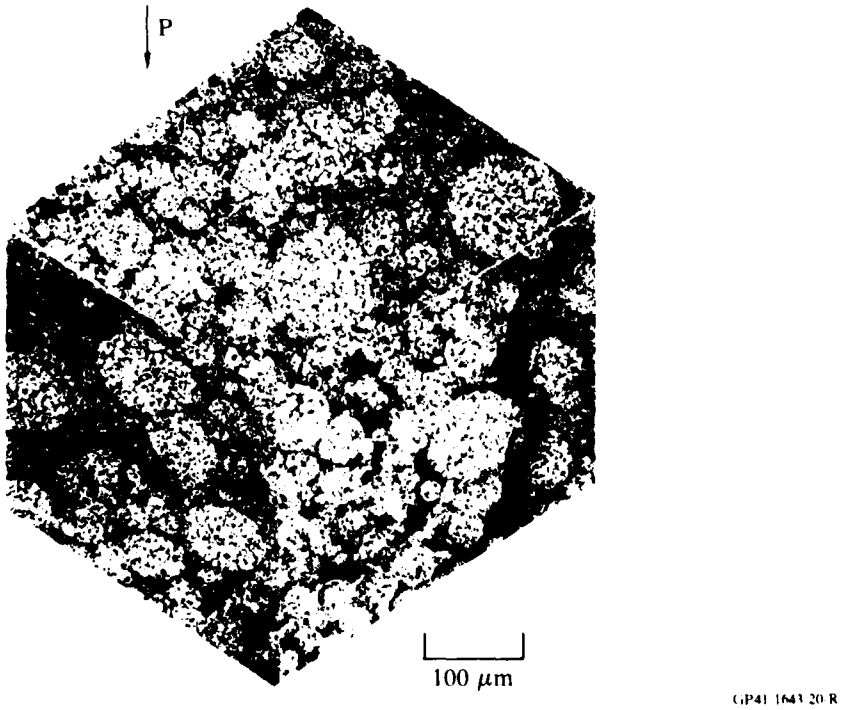

Figure 20. Optical micrographs of Al-3Li-1Cu-1Mg-0.2Zr alloy powder compacts consolidated by uniaxial pressing at 400°C.

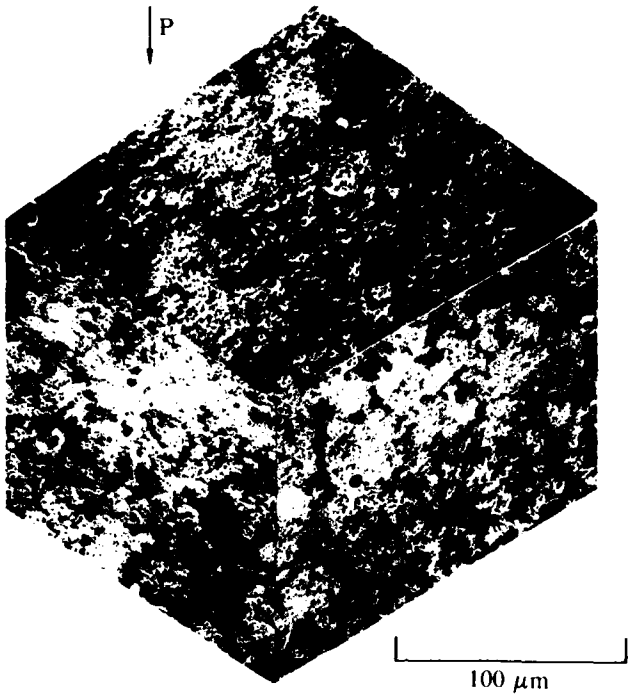

GP41 1643 21-R

Figure 21. Optical micrographs of Al-8Fe-7Ce alloy powder compacts consolidated by uniaxial pressing at 400°C.

gives rise to interparticle shearing and breakdown of prior particle boundaries, thus promoting interparticle bonding. The extent of densification and plastic deformation and the resultant microstructures produced during extrusion are related to the temperature and strain-rate sensitivity of flow stress of the material.

With the objectives of determining interrelationships between material flow properties and extrusion process variables and selecting extrusion process variables for large-size powder extrusions, laboratory-scale extrusions were prepared and evaluated. Hot-pressed, 12.5-mm-diameter, 10-mm-long, cylindrical aluminum powder compacts were extruded into 3.2-mm-diameter cylindrical rods in a stainless steel die with 16:1 cross-sectional area reduction ratio and ram displacement rates of 0.02 to 0.16 cm/s.

The extrusion rate dependence of flow stress for Al and Al-Li-Cu-Mg-0.2Zr extruded at 400°C is shown in Figure 23. At extrusion rates < 0.04 cm/s, flow stress is insensitive to extrusion rate in aluminum, but at larger extrusion rates, the flow stress increases with extrusion rate with a rate sensitivity of 0.2. The Al-Li-Cu-Mg-Zr alloy, however, exhibits rate sensitivity ≈ 0.2 at all extrusion rates from 0.02 to 0.16 cm/s.

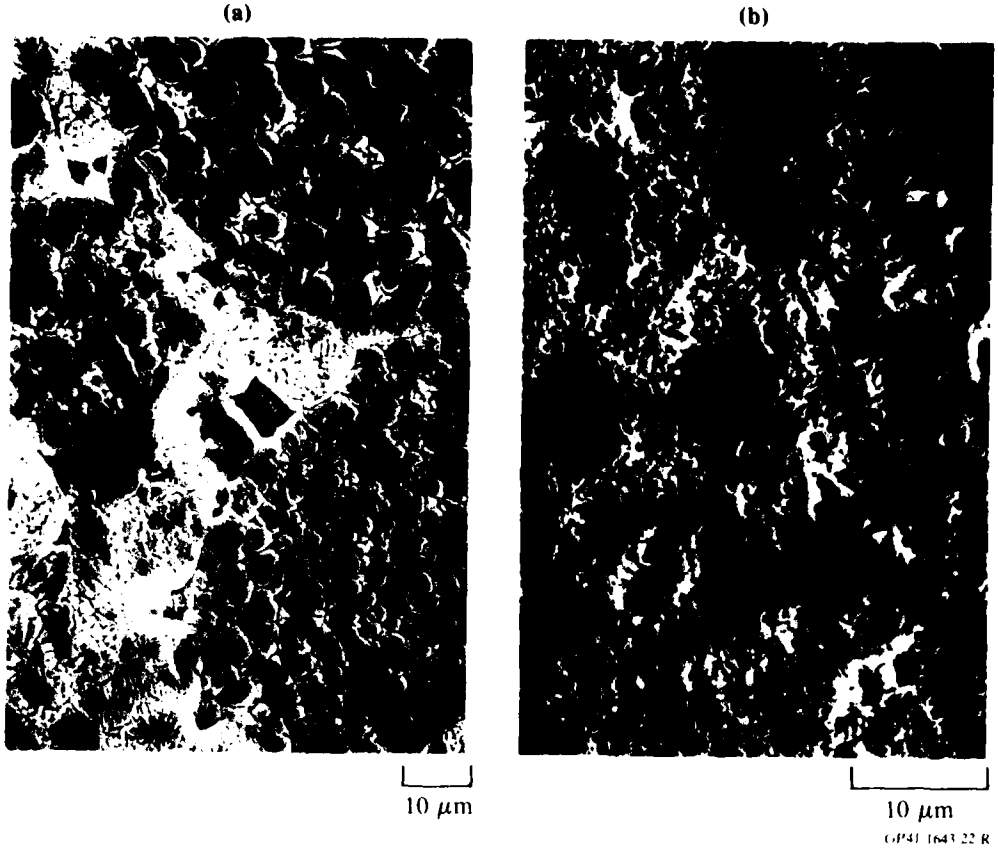

Figure 22. High-magnification scanning electron micrographs of (a) Al-3Li-1Cu-1Mg-0.2Zr and (b) Al-8Fe-7Ce alloy powder compacts consolidated by uniaxial pressing at 400°C.

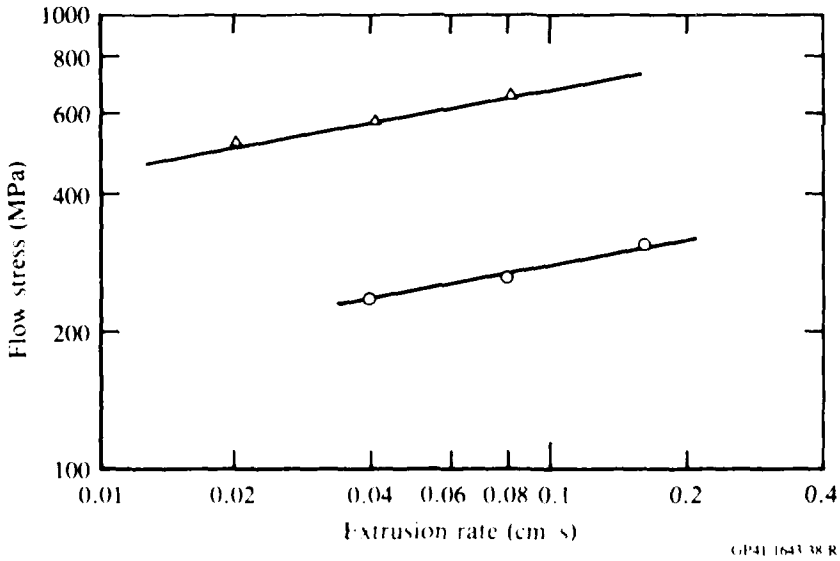

Figure 23. Variation of flow stress with extrusion rate of (○) aluminum and (△) Al-3Li-1Cu-1Mg-0.2Zr powders extruded at 400°C.

The microstructures of aluminum powder compacts extruded at 400°C at ram displacement rates of 0.01, 0.04, 0.08, and 0.16 cm/s are shown in Figures 24a-24d. The specimen extruded at 0.01 cm/s has large numbers of voids at the interparticle boundaries. The powder particles are elongated in the extrusion direction. The original particle boundaries are clearly seen, indicative of poor interparticle bonding. The microstructure resembles that of a hot-pressed Al powder compact (compare Figures 24a and 19). In specimens extruded at higher displacement rates, complete interparticle bonding occurred without a trace of prior interparticle boundaries. Dynamic recrystallization resulted in recrystallized grain structures with grains elongated in the extrusion direction. The grain size in the plane perpendicular to extrusion direction decreases from ~ 10 μm at 0.04 cm/s to ~ 5 μm at 0.16 cm/s.

The Al-Li-Cu-Mg-Zr alloy extruded at 0.02 cm/s shows the original particle boundaries and the dendritic and cellular microstructure similar to those observed in hot-pressed alloy (Figure 25a). However, the specimen extruded at 0.08 cm/s reveals complete bonding without any evidence of interparticle boundaries (Figure 25b). In contrast to the recrystallized microstructures observed in Al, the Al-Li based alloy exhibits a recovered microstructure. The recrystallized 5- to 10-μm grain structure in extruded Al and recovered 1- to 2-μm subgrains in extruded Al-Li based alloys are shown in transmission electron micrographs of Figures 26a and 26b.

3.3.4 Explosive Compaction of Aluminum Alloys

Under the currently employed static-consolidation conditions (high temperatures and pressures for several hours), certain amounts of recrystallization, grain growth, phase change, precipitation, and segregation are inevitable. Many of these microstructural changes diminish the effectiveness of heat treatments in controlling mechanical properties after consolidation. Finally, the ever-present surface oxide on individual Al-alloy particles is not easily broken and dispersed in the static-consolidation process, with the result that interparticle bonding is poor. Dynamic consolidation by explosive compaction is being investigated by MDRL under the McDonnell Douglas Independent Research and Development (IRAD) program[10,11] to determine optimum process parameters for explosive consolidation of aluminum-lithium alloys. Research under this contract program will focus on the determination of the effects of material

GP41 1643 23 R

Figure 24. Optical micrographs of aluminum powder compacts extruded at 400°C at extrusion rates of (a) 0.01 cm/s, (b) 0.04 cm/s, (c) 0.08 cm/s, and (d) 0.16 cm/s.

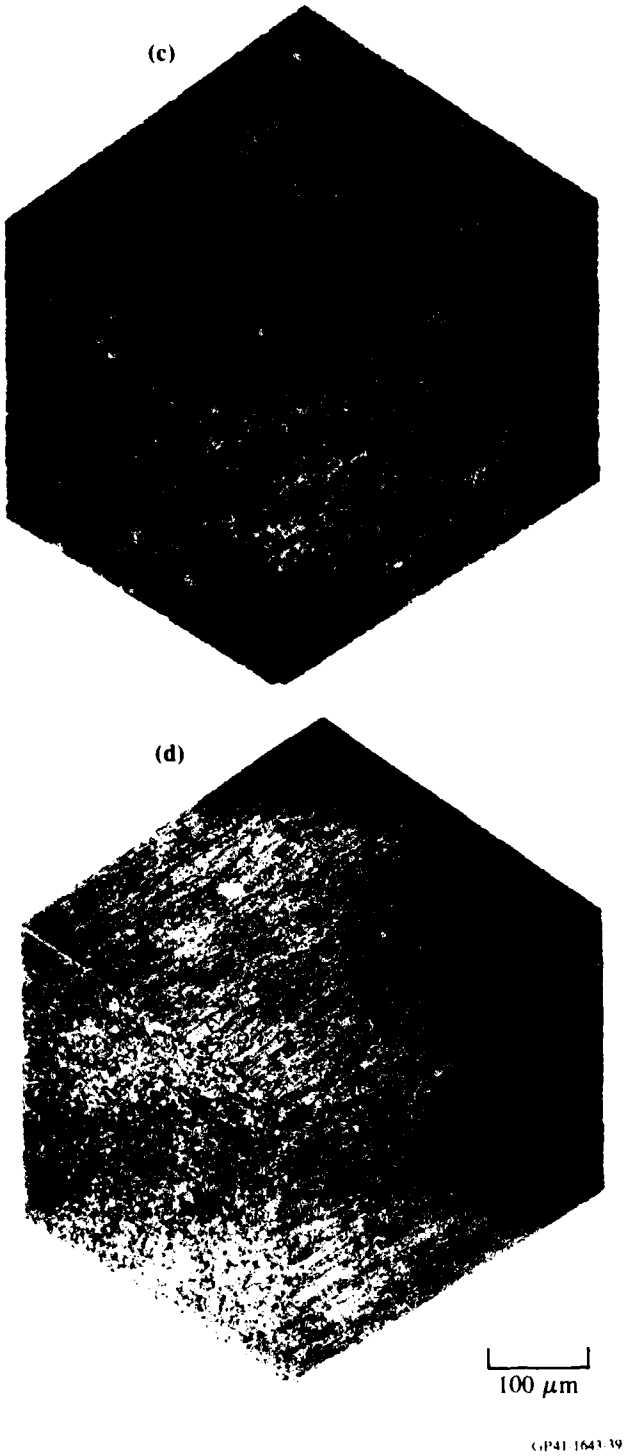

Figure 24. (Concluded)

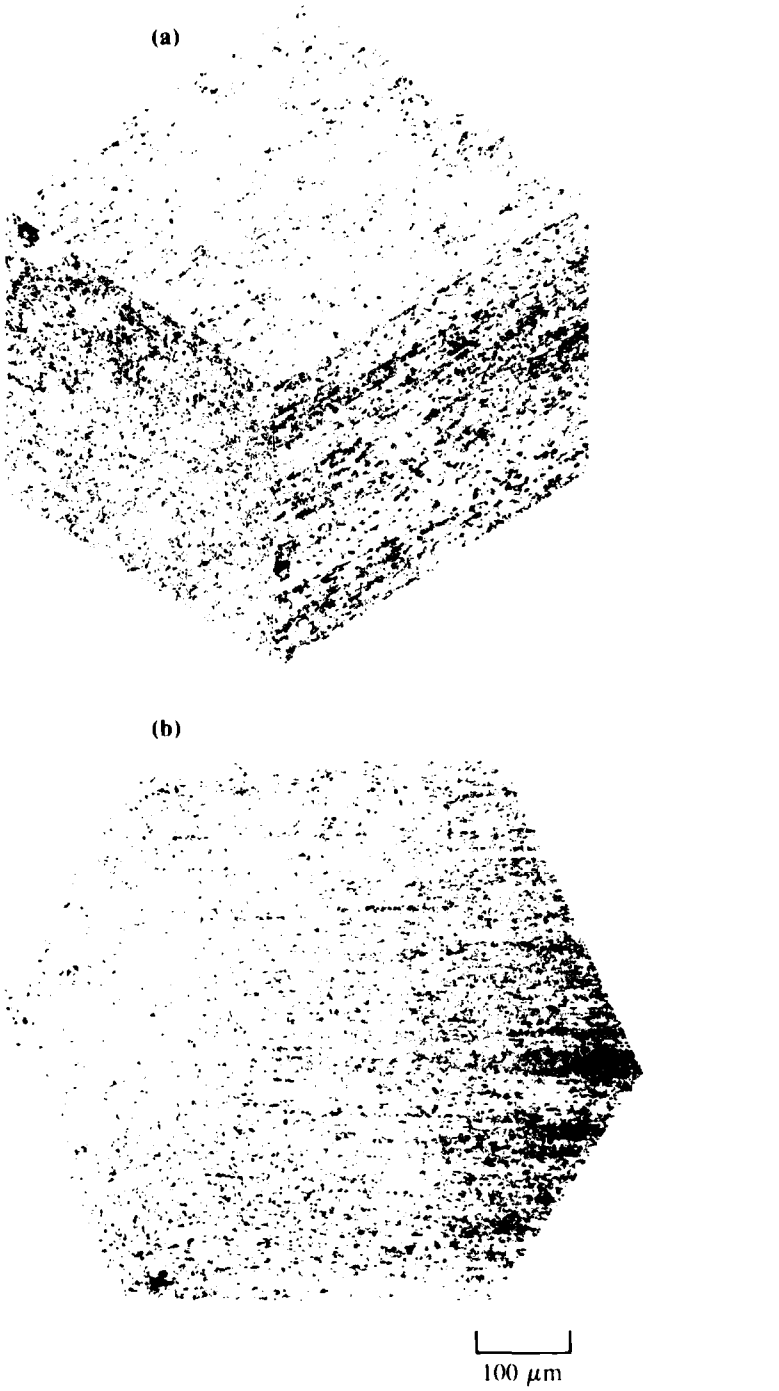

Figure 25. Optical micrographs of Al-3Li-1Cu-1Mg-0.2Zr alloy powder compacts extruded at 400°C at extrusion rates of (a) 0.02 cm/s and (b) 0.08 cm/s.

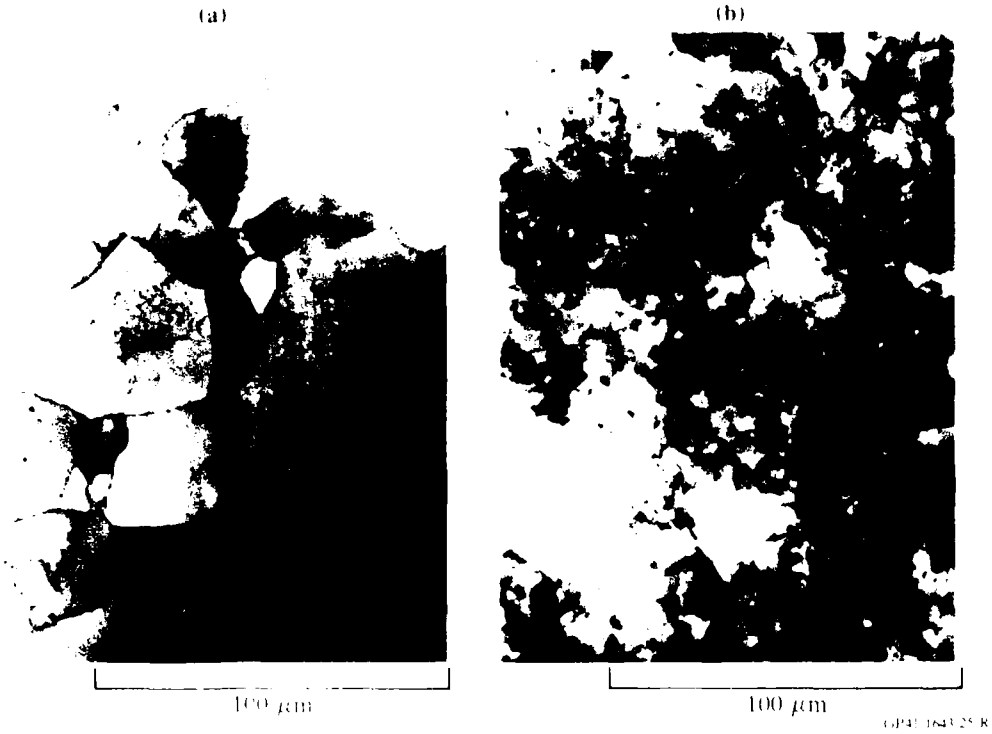

Figure 26. Transmission electron micrographs of (a) aluminum and (b) Al-3Li-1Cu-1Mg-0.2Zr powder compacts extruded at 400° C at an extrusion rate of 0.08 cm/s.

variables on densification and interparticle bonding during explosive consolidation. 99.9% Al, and Al-8Fe-7Ce alloys having large differences in hardness, flow stress, and work-hardening rate have been selected for the study.

A schematic of the explosive compaction arrangement is shown in Figure 27. Compaction begins as the shock wave from a burning explosive travels through the top-end plug of the container into the metal powder pack. The compacting pressure generated by the shock wave violently agitates and compresses the individual powder particles in the pack. Large amounts of energy released by these reactions produce an instantaneous peak pressure which immediately readjusts itself to a more stable value at the Chapman-Jouquet (C-J) point where all chemical reactions cease (Figure 27). Behind the C-J point, pressure dissipates relatively slowly through the expansion of the product gas. While the pressure dissipation is occurring, an inward pressure is exerted on the powder compact. Depending on the type of explosives, a high-pressure pulse (multiples of GPa) can be created. The pressure at the C-J

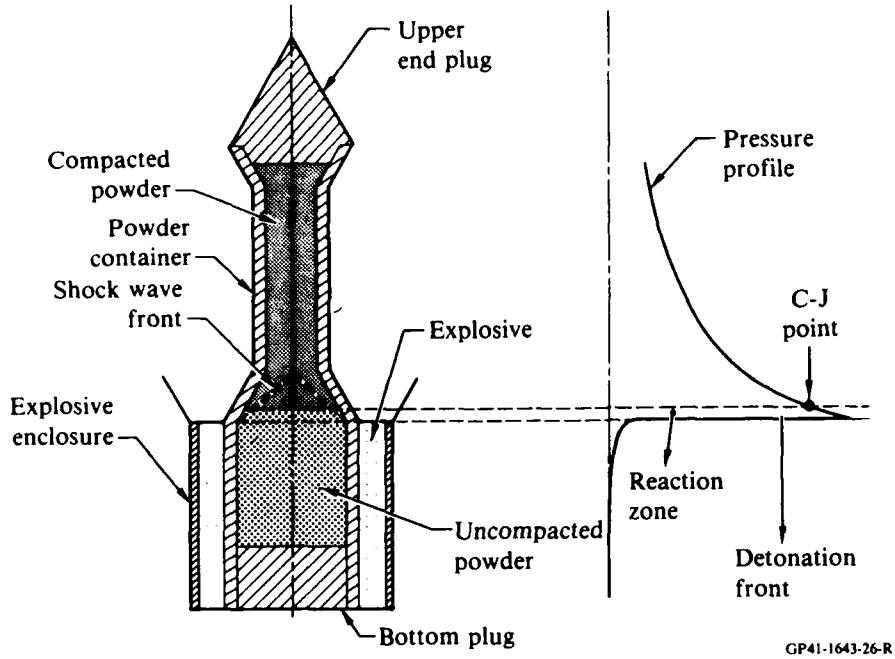

Figure 27. High-energy-rate consolidation of rapid solidification processed (RSP) alloys.

point P_{C-J} (the compaction pressure) may be estimated based on one-dimensional shock theory[12,13] by

$$P_{C-J} = \frac{\rho_e V^2}{\gamma + 1} , \tag{9}$$

where ρ_e = density of the explosive powder, γ = specific heat ratio of the product gas, and V = detonation velocity. The detonation velocity V is related to the heat released from the explosives Q by

$$V^2 = 2Q(\gamma^2 - 1) . \tag{10}$$

V and Q can be measured experimentally, and γ can thus be determined and the compaction pressure P_{C-J} calculated. Values of P_{C-J} for most explosives ranges from 1-60 GPa. The compaction pressures can be varied by varying the explosives. The high-energy density behind the shock can melt the particle surface layers to form strong interparticle bonds and leave the bulk microstructure unaltered. When the shock wave reaches the lower-end plug, the compacting pressure is further increased on the shock wave reflection.

Compacting pressures > 1 GPa are required to achieve 100% densification of aluminum powders.

Explosive compaction experiments have been started. Based on MDRL IRAD results,[10,11] detonation velocities of 2-3 km/s have been selected for the initial set of experiments. The powders were packed in 3.2-cm-diameter, 14-cm-long, mild steel cylinders. The packing sequence consisted of evacuating the cylinder and vibrating the powder for 24 h. A 0.64-cm-diameter 2024Al-alloy core rod was used to reflect the inward compression wave into an outward compression wave and thus prevent radial cracking. The powder packs have been sent to New Mexico Institute of Mining and Technology for explosive detonations.

4. PUBLICATIONS AND PRESENTATIONS RESULTING FROM AFOSR SUPPORT

1. S. M. L. Sastry, T. C. Peng, and J. E. O'Neal, Novel Consolidation Methods for Rapidly Solidified Aluminum-Lithium Alloys, Presented in the Symposium on Structural Aluminum Alloys for Aerospace Applications, TMS-AIME Fall Meeting, Detroit, MI, September 16-20, 1984.
2. S. M. L. Sastry, R. J. Lederich, and J. E. O'Neal, High-Temperature Flow Characteristics of Al-Li-Zr Alloys, TMS-AIME Annual Meeting, Los Angeles, CA, February 26-March 1, 1984.
3. Deformation Behavior of Rapidly Solidified Al-3Li Based Alloys, Invited talk presented in the Department of Metallurgy and Materials Science, University of Toronto, Canada, June 20, 1984.

5. LIST OF PERSONNEL

The following MDRL personnel participated in this AFOSR-funded research:

S. M. L. Sastry - Senior Scientist

T. C. Peng - Scientist

D. M. Bowden - Research Scientist

J. E. O'Neal - Scientist

6. COUPLING ACTIVITIES WITH GROUPS DOING RELATED RESEARCH

1. Briefing on the objectives and approach of the program to AFWAL-ML personnel Dr. T. Ronald (LLS), Mr. W. Griffith (LLS), Lt. J. Adkins (LLS), and Dr. H. Gegel (LLM) at AFWAL-ML, Wright-Patterson Air Force Base, OH, 14 February 1984.
2. Briefing on the objectives, approach, and progress on MDRL/AFOSR Al-Li Alloy Powder Consolidation Research to Mr. Joe Collins (NASC) and Mr. A. P. Divecha (NSWC) on 14 August 1984.
3. Discussion with Prof. H. Fraser (University of Illinois, Urbana-Champaign) on Microstructures of Explosively Consolidated Al Alloy Powders, September 1983.

7. REFERENCES

1. S. M. L. Sastry, P. J. Meschter, J. E. O'Neal, and K. K. Sankaran, Microstructure and Properties of Powder Processed Aluminum Lithium Alloys, AFOSR Contract No. F49620-79-C-0039, Final Report, MDC Q0778, May 1982.
2. R. E. Lewis, D. Webster, and I. G. Palmer, A Feasibility Study for Development of Structural Aluminum Alloys from Rapidly Solidified Powders for Aerospace Structural Applications, AFML-TR-78-102, July 1978.
3. W. M. Griffith, R. E. Sanders, Jr., and G. J. Hildeman, Elevated Temperature Aluminum Alloys for Aerospace Applications, in High-Strength Powder Metallurgy Aluminum Alloys, M. J. Koczak and G. J. Hildeman, eds. (TMS-AIME, Warrendale, PA, 1982), p. 209.
4. J. P. Lyle, Jr. and W. S. Cebulak, Properties of High-Strength Aluminum P/M Products, Metals Eng. Quarterly 14 (1), 52 (1974).
5. A. P. Divecha and S. G. Fishman, Mechanical Properties of Silicon-Carbide Reinforced Aluminum, New Matl. 3, 351 (1979).
6. S. L. Langenbec, Elevated Temperature Aluminum Alloy Development, Interim Report, Air Force Contract F33615-81-C-5096, AFWAL/MLLS, W-PAFB, OH, December 1982.
7. R. W. Heckel, A New Approach to the Study of Powder Compaction, Progress in Powder Met. 17, 66 (1961).
8. A. K. Mukherjee, High-Temperature Creep, in Treatise on Materials Science and Technology, Vol. 6, R. J. Arsenault, ed. (Academic Press, New York, 1975), p. 163.
9. R. L. Coble, Diffusion Models for Hot Pressing with Surface Energy and Pressure Effects as Driving Forces, J. Appl. Phys. 41, 4798 (1970).
10. McDonnell Douglas Research Laboratories, Independent Research and Development Programs, 1983, MDC Q0866-4, 134001 and 1984, MDC Q0871-4, 144001.
11. T. C. Peng, S. M. L. Sastry, and J. E. O'Neal, Explosive Compaction of Rapidly Solidified Aluminum-Alloy Powders, Met. Trans. (submitted).
12. V. D. Linse, ed., Dynamic Compaction of Metal and Ceramic Powders, National Academy of Sciences Report NMAB-394, Washington, DC, 1983.
13. O. V. Roman and V. G. Gorobtsov, Fundamentals of Explosive Compaction of Powders, in Shock Waves and High-Strain Rate Phenomena in Metals, M. A. Meyers and L. E. Murr, eds. (Plenum Press, 1981), p. 829.

END

FILMED

5-85

DTIC